Development of an Efficient and Accurate Laser Cladding Strategy by Using Feed Rate-Based Control Method

By

GENG LI

DISSERTATION

Submitted in partial satisfaction of the requirements for the degree of

DOCTOR OF PHILOSOPHY

in

Mechanical and Aerospace Engineering

in the

OFFICE OF GRADUATE STUDIES

of the

UNIVERSITY OF CALIFORNIA

DAVIS

Approved:

_____

Masakazu Soshi, Chair

_____

Nesrin Sarigul-Klijn

_____

Mohamad M. Hafez

Committee in Charge

2022

Table of Contents

Page

Acknowledgments

Thank you to my family mom, dad for their love and understanding. As their son, I cannot give anything in return but love and understanding.

I would like to extend my special gratitude to Prof. Soshi for his guidance, patience and continuous support. Prof Soshi helps me go through every aspect of the academic work. I could not imagine how my graduate life would be without Prof. Soshi's generous help. I also could not expect anything better from my advisor.

I wish to express my appreciation to Prof. Sarigul-Klijn and Prof. Hafez for reviewing this dissertation and their valuable comments.

Additionally, I would like to thank DMG Mori for the invaluable help and support. This research is also not possible without the selfless help from my friends and colleagues in the lab.

Geng Li
December 2021
Mechanical and Aerospace Engineering

Abstract

Directed energy deposition (DED) is an additive manufacturing process which can be used to produce customized complicated parts with less cost compared with the conventional subtractive manufacturing method. However, the parts produced by DED can be deformed severely due to excessive heat accumulation. The input energy, typically laser and electron beam, is commonly regulated in many literatures to minimize the deformation based on the temperature information of the existing clad. Although the energy input control method is proved effective in reducing the deformation, the productivity of DED process is not increased.

In this dissertation, a feed rate-based fuzzy logic controller is proposed to maintain geometric consistency and increase the production rate at the same time. The geometric consistency and productivity are effectively improved, through numerical simulation and experiments of thin wall and square blocks in stainless steel 316L. However, feed rate control is not functional for small parts without sufficient cooling time. Therefore, a series of square blocks with various dimensions are modeled to test the threshold for choosing the proper control method. Additionally, a python program is developed to accelerate the simulation speed.

List of Figures

Page

List of Tables

Page

Nomenclature

AM	Additive manufacturing
DED	Directed energy deposition
PBF	Powder bed fusion
EF	Energy flux
PF	Power flux
d	Laser spot diameter
q	Laser power
q_{in}	Laser energy flowing into the melt pool
k	Conductivity
h	Convection coefficient
A	Top surface area of melt pool
ϵ	Emissivity of the melt pool
σ	Stephan-Boltzman constant
T_∞	Environmental temperature
V_p	Volume of added powder
T_{0_p}	Initial temperature of the powder prior to incorporation into the melt pool
V_s	Volume of remelted portion of the substrate

T_{0_s}	Initial temperature of the remelted portion of the substrate
T_{liq}	Liquidus temperature
T_{sol}	Solidus temperature
c	Specific heat
c_s	specific heats of solid state
c_l	specific heats of liquid state
ΔH_f	Latent heat of fusion
T_{ss}	Steady state temperature
v	Feed rate
$\dot{m}$	Powder flow rate
t	Time
Δt	Time increment
ρ	Density
U	Internal energy
T	Current temperature
δT	Temperature variance of two consecutive iterations
N	Nodal direction
q_v	External volume energy source

q_s	External surface energy source
n_{total}	Total number of the increments
t_{sim}	Simulation running time
t_{incre}	Actual time to complete an increment
t_{iter}	Actual time to complete each iteration
I	Number of iterations in an increment
Δl	Typical element dimension
A_t	Attenuation rate
q_a	Attenuated laser power
q_l	Incident laser power
D_p	Diameter of the powder flow
r_p	Radius of the powder particles
v_p	Powder particle velocity
θ	Inclination angle relative to the surface normal
α	Laser absorption rate
r	Distance from laser spot center to nodal location
s_C	Cosine similarity
$T_{current}$	Current clad top surface median temperature

$T_{previous}$	Median temperature of previous layer
$T_{objective}$	Objective temperature
$\mu(x)$	Probability of the laser power increment
a	Active field of heat transfer
r_{max}^{a}	Largest residual in balance equation for field a
R_{n}^{a}	Criterion for residual heat flux
$\tilde{q}^{a}$	Overall time-averaged value of the heat flux for field a
c_{max}^{a}	Largest correction to nodal variable
C_{n}^{a}	Criterion for temperature correction
Δu_{max}^{a}	Largest nodal temperature change

1. Introduction

1.1 Directed Energy Deposition Background

1.1.1 Additive Manufacturing

Additive manufacturing (AM) is the collection of methods by which parts are built by adding material to the existing parts. AM is capable of fast producing customized parts from three-dimensional models and does not require molds. Therefore, it is particularly useful for making a small batch of products and parts with complicated geometry.

The early additive manufacturing machine can track back to the 1980s, the AM technique was mostly used for filament deposition, which is still commonly seen in today's market. In this technique, plastic material was extruded and fused to form the desired shape. Metal AM methods have also been developed since then, including powder bed fusion (PBF) and directed energy deposition (DED).

1.1.2 Power Bed Fusion (PBF)

Powder bed fusion is a type of metal AM method, which uses thermal energy source to selectively melt a regional metal powder. In PBF, the metal powder with pre-determined thickness is pre-deposited on the building platform. After the metal powder is selectively melted, the building platform is lowered, and the top surface is covered by newly added metal powder. The part is built by repeating the selective melting and depositing process, figure 1.

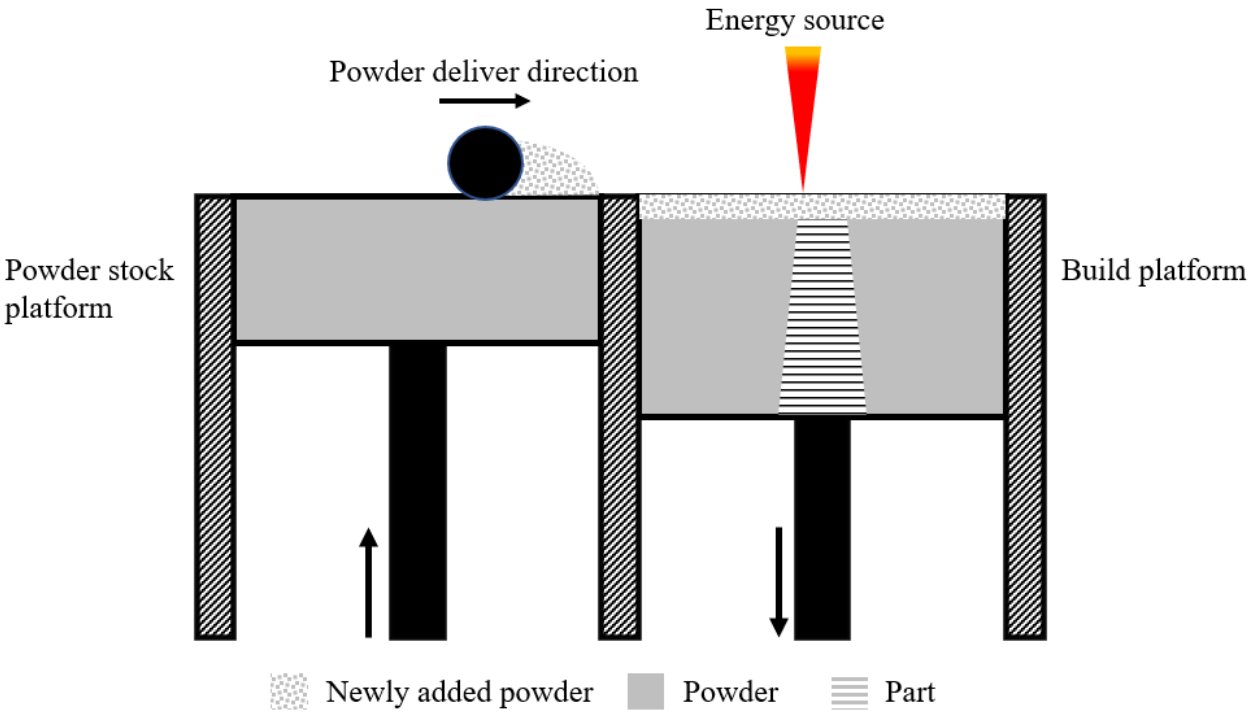

Figure 1. Powder bed fusion process

Both laser and electron beam energy sources are typically used in the PBF method. The electron beam is particularly suitable for processing brittle materials due to their low thermal expansion and contraction behavior. Cracks can be formed due to the residual stress if the cooling rate is too fast for brittle material. This issue can be solved by electron beam melting method (EBM). In EBM, the powder bed is heated to reduce the cooling rate by increasing the high surrounding powder temperature. Although cracks can be avoided by low cooling rate, the cooling time can be rather time-consuming. The part cannot be removed from the chamber after the cladding process is finished until the chamber reaches room temperature, which usually takes several hours [1].

1.1.3 DED

Unlike PBF, laser energy and material are applied to the substrate or basement simultaneously along with the inert gas in DED, presented in figure 2. Substrate is the support structure in AM

and is generally required for the part to build on. Melt pool is created under the laser power and metal powder is fed directly to the melt pool. The melt pool is composed of the newly added metal powder and part of the remelting substrate or existing layer. Like PBF, the DED part is built in a layer-by-layer manner. However, the material is directly deposited on the working surface in DED which also has the advantage of lower dilution rate, good metallurgical bonds, and smaller heat-affected zone compared with PBF. Therefore, DED can be used to repair damaged parts by coating onto the existing part [2]. Both metal wire and powder are commonly used in DED process. Generally, the metal wire is relatively material-efficient because of the high material capture rate due to the nature of the wire form [3]. Compared with wire, metal powder is more expensive and less efficient since not all metal powder can be captured by melt pool. However, with a delicately designed powder recycle system, a substantial amount of metal powder can be reused. The powder DED system also has advantages of cladding efficiency and accuracy over wire systems.

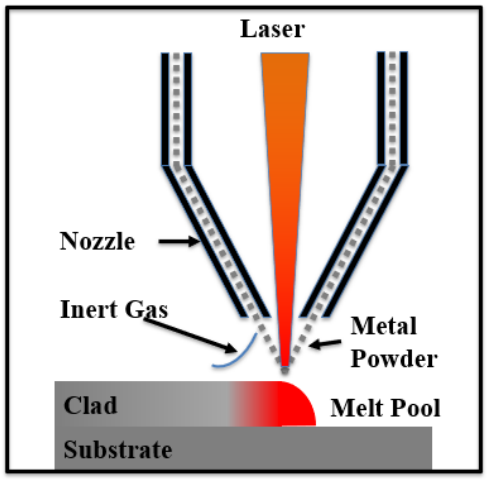

Figure 2. DED with laser energy source and metal powder material

Both metal AM methods have strengths and challenges. A part built by PBF can have finer geometric details than the part built by DED, but the size is limited to the building platform size [4]. On the other hand, a part built by DED is not restricted by machine size, but an inert gas

environment is usually required to reduce the oxidization rate in the cladding process [1]. DED is also capable of mixing multi-metal powder for the fabrication of functional-graded material [5], which has various applications such as bone replacement and space vehicle. Porosity is one of the commonly shared limiting factors of AM. However, research shows that, with carefully designed DED parameters, porosity can be controlled as well as other material properties such as yield strength and tensile strength [6].

1.1.2 Directed Energy Deposition Process

1.1.2.1 Major DED Parameters

In the DED process, not only porosity and material strength can be affected by cladding parameters but also clad geometry is influenced by the cladding parameters. ~~There are many important parameters in DED process, such as t~~The laser spot diameter, the distance between deposition head and melt pool, and the powder particle size~~, etc~~ are among the most important process parameters. Melt pool size is highly related to the laser spot diameter. Study shows that porosity has a positive correlation with the powder particle size [7]. However, this study is focused on only three cladding parameters, which are laser power, deposition feed rate, and powder flow rate. All the other parameters are assumed to be constant.

It has been revealed in many researches that these three parameters have a significant impact on clad geometry. Meanwhile, a study shows that clad width is more sensitive to laser power and feed rate rather than powder flow rate [8]. Similarly, it also has been shown in research that if the ratio of powder mass flow rate to feed rate is constant, the cross-section area of the clad is also invariant [9]. Therefore, the combination of the cladding parameters is usually used to reveal the relationship between cladding parameters and geometry.

The intensity of the energy source of different DED machines widely varies from 200W to 15kW. Despite the type and intensity of energy source difference of the DED machine, the purpose of the energy source is to melt a certain amount of metal material in a short period. To better describe how strong the energy source is, deposition feed rate and laser spot diameter should be considered as well. Therefore, the energy flux, EF, of the laser into the melt pool is the ratio of laser power, q, and the product of laser spot diameter, d, and deposition feed rate, f, presented as:

$$EF = \frac{q}{d \cdot f} \tag{1}$$

Similarly, powder flux, PF, is the ratio of the mass of powder flow rate, $\dot{m}$, and the product of the laser spot diameter and deposition feed rate:

$$PF = \frac{\dot{m}}{d \cdot f} \tag{2}$$

EF has SI units of $\mathrm{J/m^2}$ and PF has units of kg/m^2. The powder flux is also known as the mass flow rate.

The PF describes the amount of powder added to the clad in unit length and time, assuming the energy source is sufficient to melt input powder and substrate. It has been claimed by several researchers that the clad height has a linear relationship with powder flux [9]–[11].

In the Advanced Research for Manufacturing Systems (ARMS) laboratory at UC Davis, the relationship between clad geometry and flux is obtained from comprehensive experiments [12]. The clad height has a linear relationship with the powder flux, which is also presented in the equation below.

$$h = 1.025 \cdot PF \tag{3}$$

where h is the clad height. Similarly, the equation below describes the relationship between energy flux and clad width.

$$w = 3.10(1 - \exp(-1.25 \cdot EF)) \quad (4)$$

Where w is the clad width. Although the variance of the data which generated the relationship equations is not trivial, especially the variance in figure 3.b, these equations still can be used to estimate the clad dimension for simulations.

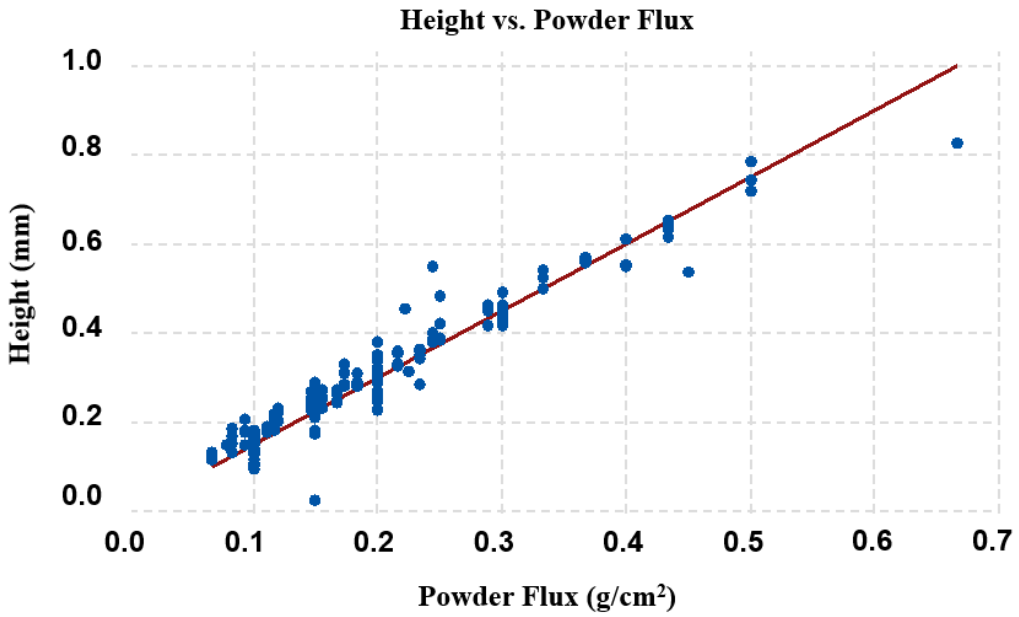

a)

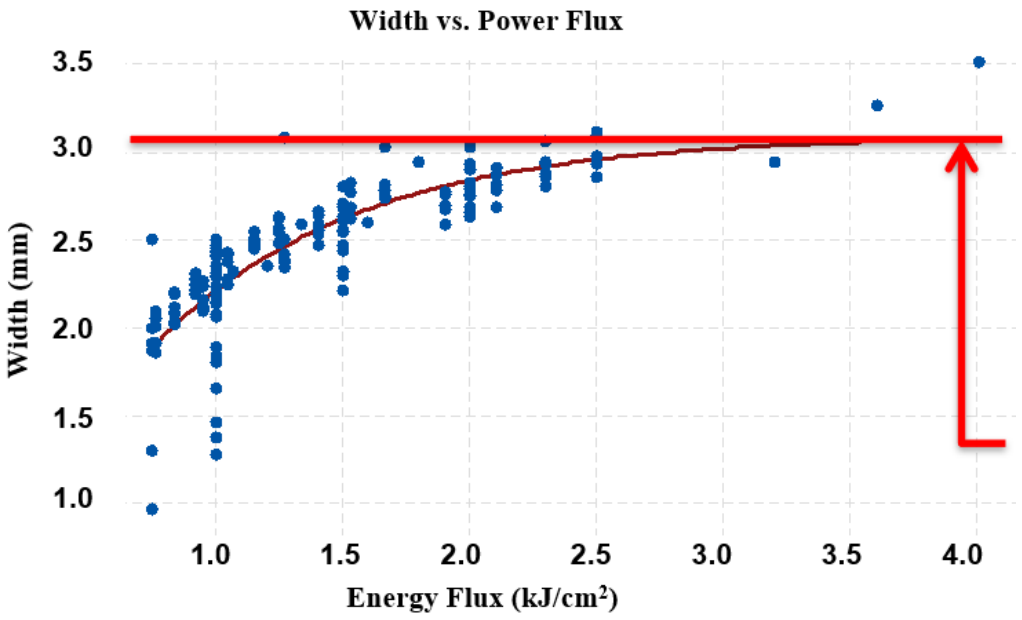

b)

Figure 3. a) Linear regression for clad height and powder flux; b) Exponential regression for clad width and energy flux

1.1.2.2 DED Energy Balance

The relationship between the clad width and EF or substrate temperature is rather complicated. To better understand the relationship of the clad width and cladding parameters, the energy balance of the melt pool is presented in the equation below:

$$q_{in} = -k\vec{\nabla}T + hA(t - T_{\infty}) + \epsilon\sigma A(T^4 - T_{\infty}^4) + \rho V_p \left(\int_{T_{0_p}}^{T_{liq}} c_s dT + \Delta H_f + \int_{T_{sol}}^{T} c_l dT \right) + \rho V_s \left(\int_{T_{0_s}}^{T_{liq}} c_s dT + \Delta H_f + \int_{T_{sol}}^{T} c_l dT \right) \quad (5)$$

Where q_{in} is the laser energy flowing into the melt pool, k is the thermal conductivity of the material, h is the convection coefficient, A is the surface area of the melt pool, ϵ is the emissivity of the melt pool, σ is the Stephan-Boltzman constant, T_∞ is the environmental temperature, ρ is the material density, V_p is the volume of added material, T_{0_p} is the initial temperature of the powder prior to incorporation into the melt pool, V_s is the volume of remelted portion of the substrate, T_{0_s} is the initial temperature of the remelted portion of the substrate, T_{liq} and T_{sol} are the liquidus and solidus temperature of the material, c_s and c_l are the specific heats of the material in solid and liquid state, and ΔH_f is the latent heat of fusion. By assuming all the variables are correlated to each other, it can be concluded that increasing energy flux into the melt pool would cause an increase in the melt pool volume, area, and maximum temperature, especially in materials with low thermal diffusivity such as stainless steels, nickel alloys, and Ti-6Al-4V which are materials commonly used in DED.

1.1.3 DED Process Key Components

All the research and experiments in this study are based on a DMG Mori LaserTec 65 DED Hybrid, shown in figure 4, which is also the machine used in the cited lab member articles. Therefore, the DED key components are also based on the LaserTec 65 DED Hybrid. ~~LaserTec 65 DED Hybrid~~ The hybrid machine has both laser cladding ~~function~~ and ~~metal cutting~~ traditional milling functions on a 5-axis frame.~~, which is also known as the hybrid machine~~. The deposition nozzle is coaxial and capable of depositing homogeneous powder independent from the direction of laser deposition. Part of the DMG Mori Lastertec 65 DED Hybrid specifications are listed in table 1.

Table 1. Lasertec 65 DED Hybrid technical data [13]

Specifications	Unit	Technical data
Travel in X/Y/Z	mm	735/650/560
Laser spot diameter 1 (standard)	mm	3
Laser spot diameter 2 (optional)	mm	1.6
Milling spindle maximum speed 1 (standard)	rmp	14000
Milling spindle maximum speed 2 (optional)	rmp	20000
Maximum workpiece dimension (AM)	mm	Ø500×400
Maximum workpiece weight	kg	600

Figure 4. The DMG Mori Lasertec 65 DED Hybrid [1]

LaserTec 65 DED Hybrid has a laser unit, whose up limit is 2.5 kW. The purpose of the laser is to melt the incoming powder particles and a small portion of the substrate. As discussed before, energy flux is the laser energy input in unit distance and time. The excessive EF can lead to the quality issues such as deformation and deep melt pool into the substrate, which is also known as the 'keyhole' effect. On the other hand, insufficient EF can cause quality issues such as unmelted particles in the clad, which is harmful to the material strength.

Inert gas, also known as shield gas, is required during DED process to prevent metal powder from over-oxidation. The inert gas is supplied to the workpiece along with the laser and powder flow. Argon is used in the Lasertec 65D ~~and is also one of the commonly used inert gas in other DED machines.~~per the industry best practices.

The feedstock for Lasertec 65D is metal powder. The powder diameter size range is generally between 50-150 μm. The particle size smaller than 10 μm can compromise the flowability. On the other hand, porosity can be caused by large powder particles which entrap gas during DED process [14]. The powder flow rate in this study can be up to 35g/min.

1.2 Research Objective

1.2.1 Motivation and Goal

Although the DED has many distinct advantages, DED still shares some common challenges with other AM methods, such as poor geometric accuracy, low productivity, and porosity. The inconsistent melt pool temperature distribution is one of the important factors which can cause poor geometric accuracy [15]. Research has been done to improve geometry accuracy by controlling the melt pool temperature in real-time. The laser power is generally the only control variable to maintain melt pool temperature and size during cladding, while feed rate and powder flow rate remain constant.

The feed rate-based control is rarely studied, even though controlling the feed rate can also manage the energy flux to achieve geometry consistency and improve productivity at the same time. ~~Furthermore, the DED machines, such as LaserTec 65 DED Hybrid, can operate at a higher speed, 4000mm/min, than the recommended value, 1000mm/min (Autoridad Nacional del Servicio Civil, 2021). The feasibility of utilizing the maximum machine capacity is inspired by the large gap~~

~~between the recommendation feed rate and DED machine capability.~~ This method can effectively maintain a consistent clad geometry, while also increasing total process feed rate. Improivng the feed rate of the DED process represents a large untapped improvement to productivity, as DED machines are usually capable of feed rates much higher than the cladding feed rates recommended by the manufacturer. For example, the LaserTec machine is capable of 4000mm/min, in contrast to the manufacturer recommended 1000mm/min rate to be used while cladding. [12].

Therefore, the goal of this study is to develop a strategy to improve the DED productivity and geometric accuracy at the same time by energy management mainly via controlling machine feed rate. The effectiveness of the proposed feed rate-based method is validated by numerical simulation and experiments. The limitations of the proposed method are also investigated, and ~~the~~ countermeasures ~~is~~ are discussed.

1.2.2 Approach

Due to heat accumulation in the substrate, it is common to reduce the laser power to control the clad width, especially in the case of long depositions. By reducing the laser power while maintaining the feed rate and laser spot size, the EF value is decreased. Several closed-loop controllers that automatically reduce the laser power based on optically monitored melt pool morphology are available on the market to manage excessive melt pool energy accumulation to maintain clad geometric accuracy.

While controlling laser power based on melt pool monitoring has shown to be effective at controlling clad width throughout a multi-layer DED part, a reduction of EF can also be achieved by increasing deposition feed rate, assuming the laser power is constant. If the deposition feed rate is increased, the powder mass flow rate must also be increased to maintain a constant PF as well

as the clad height. By scaling the powder mass flow rate and deposition head feed rate while holding laser power constant the melt pool energy and clad dimensions can be maintained while simultaneously reducing DED cycle time, thus increasing productivity. By utilizing a Dynamic Powder Splitting System, which is implanted next to the laser head and capable of controlling powder flow in real-time with a bandwidth of <0.5 s, it is possible to implement feed rate-based melt pool energy control to simultaneously reduce DED part width variation, maintain overall part geometry, and reduce deposition cycle time.

However, the cooling time of the substrate is also reduced with the cladding time due to the increasing feeding rate. The substrate temperature will increase because of the reduced cooling time. According to equation (5), V_s will also increase due to the increased T_{0_s}, assuming other terms are invariant. Thus, the increasing substrate temperature will compensate for the decreased input EF. The feed rate should be carefully designed to avoid excessive melt pool energy due to increasing substrate temperature, otherwise reducing the energy flux ~~is not~~ would not be enough to keep clad geometry from deformingation. ~~Because~~ T_{0_s} is less sensitive to the reduced cooling time for ~~the~~ a large workpiece than ~~the~~ for a small workpiece ~~,~~ due to the nature of the cooling rate curve ~~,~~ so the workpiece size is a crucial parameter to balance the increasing substrate temperature and reduced EF. Therefore, the threshold of the workpiece size will be studied to best utilize the machine capacity within the workpiece size tolerance.

In ARMS lab, the relationship between single clad layer geometry and cladding parameters is revealed by comprehensive experiments as referenced before [12]. However, the relationship between clad geometry and cladding parameter of a multi-layer geometry is difficult to be obtained by experiment because the surface temperature of each layer is inconsistent and hard to be tracked during cladding. Thus, a numerical model is built in ABAQUS to investigate the relationship

between surface temperature and cladding parameters by assuming the clad geometry is consistent in steady-state. The steady-state in DED can be described as: a steady state is reached when the surface temperature distribution of the current layer is the same as the previous layer given the same cladding parameters. The steady-state of the cladding process largely depends on the clad geometry and cladding parameters. Severe deformation can happen if the recommended cladding parameters are applied to a small workpiece, but the same cladding parameters can result in consistent geometry if applied to a large workpiece. It is beneficial to know the relationship among cladding parameters, steady-state temperature, and clad geometry to improve the cladding efficiency as well as maintain clad geometry consistency. The relationship equation below can be generated from simulation data by using proper regression.

$$T_{ss} = f(l_n, q, v, \dot{m}) \tag{7}$$

Where T_{ss} is the steady-state temperature, l_n is the normalized clad size, q is the laser power, v is the feed rate, $\dot{m}$ is the powder flow rate. Normalized clad size varies depending on the shape of the clad. For example, if the normalized size of a circular clad is the diameter; the normalized size of a polygon is the ratio of perimeter and the number of sides.

In the numerical simulation, the three major cladding parameters, laser power, feed rate, and powder flow rate, are controlled based on surface temperature to achieve the pre-determined steady-state temperature. Because the clad height has a linear relationship with the powder flux, the powder flow rate needs to be proportional to the feed rate to maintain constant clad height. As a result, the independent control variables are reduced to laser power and feed rate. Thus, equation 8 can be written as:

$$T_{ss} = f(l_n, q, v) \tag{8}$$

Compared with real-time control, the control variables in this study only change once per layer instead of every increment or time frame. The real-time control has the advantage of maintaining constant melt pool size and temperature distribution over the control method in this study, but clad geometry consistency can also be achieved by maintaining constant surface temperature distribution rather than just melt pool temperature.

However, the simulation in ABAQUS can be extremely time-consuming, especially with the numerous elements. To improve the simulation efficiency, a heat transfer model of the cladding process is developed in python to accelerate the data producing speed.

In conclusion, the efficient and accurate cladding strategy developing process can be summarized as:

- Understanding the math model of cladding process.
- Building a numerical heat transfer model to simulate the cladding process in ABAQUS.
- Developing a control method to improve the cladding efficiency and maintain clad consistency.
- Finding the relationship among cladding parameters, clad size, and steady-state temperature.
- Developing a python program to accelerate the data producing speed.

1.3 Literature Review

To better understand the DED process, many researchers have built DED process model both analytically and numerically.

1.3.1 Analytical Modelling

An analytical model of laser cladding was developed by Lalas [16] to estimate the clad width, depth, and height by taking account of feed rate and powder flow rate. Surface tension is considered the dominant effect for clad formation. For estimation of the clad characteristic, the approach has a maximum of 13% deviation for the clad width and 30% deviation for the clad height. The main source of inaccuracy is from the assumption of the geometry shape of the melt pool and measurement of the irregular clad shape, which is commonly seen in other literatures.

Another DED process model built by Picasso [17] considers the interaction between powder particles, feed rate, and major cladding parameters, such as laser power, laser beam diameter. A mathematical model is built by Pinkerton to predict the clad geometry [18]. The model is based on mass balance and energy balance of melt pool. Additionally, the profile of the melt pool is considered as an arc that reflects the surface tension forces around melt pool. The impact of feed rate on elongation of melt pool is also incorporated in the math model.

A thermal model of the multi-layer thin wall was proposed by Peyre [19]. A combination of mathematical model and numerical model is used to predict melt pool temperature distribution and melt pool geometry. The model is a 25 layers thin wall and the result is validated by temperature profile of the thin wall. Thermal couples are placed on substrate 1.5 mm and 0.5 mm from a thin wall to record the temperature history which is compared with temperature history in simulation.

1.3.2 Numerical Modelling

The theoretical models certainly reveal the connection between cladding parameters and clad geometry and can be used as a guide for process monitoring and control of the DED process.

Research by Soylemez is focused on melt pool geometry of multiple materials [20]. A numerical model is built including the effect of temperature-dependent material properties, latent heat, laser distribution, and material addition. Material addition is simulated by using model change technique.

A numerical model is proposed by Qi to predict the melt pool width and clad geometry [21]. An analytical model is built to calculate the laser power A level-set method is used to track the location of laser beam on different layers. A similar technique is implemented in this proposal as well.

1.3.3 Laser energy-based control

A closed-loop feedback control strategy is proposed by J.T.Hofman [22]. The control system uses a CMOS camera to monitor the melt pool which is processed by a software algorithm to obtain the melt pool width. The laser power is reduced up to 50% by the controller to meet the reference melt pool width. A series of single-layer clad experiments show that both melt pool width and dilution are constant over the clad.

A similar feedback controller is designed by Lijun [23]. The state-space model relating the laser power to melt pool temperature is identified experimentally using the subspace method. The melt pool temperature is tracked and compared with the reference melt pool temperature. The laser power is adjusted by the generalized predictive controller to stabilize the melt pool temperature and compensate for the lack of deposition.

The controller proposed by Yuwen et al is based on the statical analysis and optimization of the cladding parameters [24]. The influence of the cladding parameters on the clad geometry, namely clad height, width, dilution and melt pool depth is quantified in a certain range. An optimized combination of cladding parameters is also presented considering the material property and cladding time.

The relationship between cladding parameters and clad geometry has been investigated from many angles. The laser-based control method or cladding parameters optimization designed based on the relationship is commonly seen in research [25]–[29]. The clad geometry consistency has been the key point meanwhile the cladding productivity is rarely discussed.

2. DED Process modeling in Commercial Software

To fully understand the relationship between cladding parameters and clad geometry, a three-dimensional numerical model is built in commercial software, ABAQUS. The cladding process is essentially a metal powder melting and solidification process. The factors involved in the process are laser power, inert gas, and metal powder. The interaction between the laser power and metal powder can be simulated as laser power transferring from a moving energy source to the clad surface. Meanwhile, the impact of inert gas is mostly on preventing powder from oxidation rather than clad geometry. Moreover, the excessive gas pressure from the nozzle can cause surface irregularity [30]. Therefore, the cladding process can be simplified as a pure heat transfer model.

The heat transfer model of the cladding process is composed of:

- The heat transfer in the clad surface is subject to laser power.
- The energy loses from the substrate and clad due to convection and radiation.
- The conduction between melt pool and clad.
- The conduction inside the clad and substrate.

The surface tension is also important to understanding the geometry deformation. But this study is focused on improving the cladding efficiency while maintaining the geometry consistency rather than the relationship between clad geometry and the cladding parameters. Thus, surface tension is

not considered in the simulation by assuming the clad geometry will remain the same if the clad surface temperature and cladding parameters are also invariant.

Because the UI of ABAQUS does not have the utilities to provide user-defined laser track and material properties, the subroutines are necessary to model the cladding process. The subroutines can execute the instructions designed by user such as defining unique material property, specifying the location where the heat flux is applied and collecting data for output, etc. Since the subroutine is written in FORTRAN, the characteristic of FORTRAN is also discussed in this article.

Table 2. The commonly used subroutines in FORTRAN script

Subroutine	Function
UMATHU	Define material property and extract nodal information
USDFLD	Define field variables, global variables, and output data
DLFUX	Define heat flux density and location
FILM	Define film coefficient and location
GET_CP/GET_COND	Calculate the specific heat and conductivity
CONSINE	Calculate the cosine similarity
GET_DU	Calculate the internal energy increment
GET_TEMP	Calculate the temperature of next increment
SORT_TEMP	Sort the given temperature array

2.1 Heat Transfer Theory

The time-independent energy balance equation of the melt pool in the transient state is present in equation (3). Similarly, the general energy balance equation of the heat transfer process used in numerical simulation is shown in equation (1).

$$\left[\frac{1}{\Delta t}\int \rho \frac{dU}{dT}|_{t+\Delta t} dV + \int \frac{\partial N}{\partial x} k|_{t+\Delta t} dS + \int \frac{\partial h}{\partial T}(T - T_0) + h + 4\epsilon\sigma T^3 dS\right]\delta T = \int \dot{q_v} dV + \int \dot{q_s} dS - \frac{1}{\Delta t}\int \rho(U_{t+\Delta t} - U_t) dV - \int k|_t \frac{\partial T}{\partial x} dS \quad (9)$$

Where t is the time, Δt is the time increment, ρ is the material density, U is the internal energy, T is the current nodal temperature, δT is the temperature variance of two consecutive iterations,

V is the nodal volume, N is the nodal direction, k is the conductivity coefficient, h is the convection coefficient, ϵ is the emissivity factor, σ is the Stefan-Boltzmann constant, q_v is external volume energy source, q_s is the external surface energy source [31].

2.1.1 Time increment

According to equation (1), the energy balance equation tends to converge with fewer iterations if the time increment is smaller, assuming other terms are relatively invariant. The time to complete each increment is also decreasing with the number of iterations, which is time-efficient for the simulation. On the other hand, given the total cladding time in simulation is pre-determined, the simulation running time is inversely proportional to the time increment. The relationships are shown in equation (10).

$$t_{cladding} = \Delta t \cdot n_{total} \tag{10.a}$$

$$t_{sim} = n_{total} \cdot t_{incre} \tag{10.b}$$

$$t_{incre} = I \cdot t_{iter} \tag{10.c}$$

Where $t_{cladding}$ is the cladding time in simulation, n_{total} is the total number of the increments, t_{sim} is the simulation running time, t_{incre} is the actual time to complete an increment, t_{iter} is the actual time to complete each iteration, I is the number of iterations in an increment.

Therefore, time increment should be carefully designed to balance the simulation efficiency and convergence rate. In the transient heat transfer analysis, there is a general relationship between the minimum time increment and the element size.

$$\Delta t > \frac{\rho c}{6k} \Delta l^2 \tag{11}$$

Where c is the specific heat, Δl is the typical element dimension depending on the element type. If the time increment is smaller than the minimum value, spurious oscillation can appear in the solution, particularly in the simulation with vast temperature changes in a short time. The laser cladding process is a typical process with rapid temperature change. The metal powder is fused into the melt pool under the laser and solidified in a very short time. The minimum time increment can be calculated once the element dimension or mesh size is decided.

2.1.2 Mesh

In this study, the nodal coordinate of the clad should be pre-determined to enable activating the silent element. Thus, the hexahedral elements are used in preference to tetrahedron elements due to the nature of element shape, even though tetrahedron elements can provide a solution of equivalent accuracy with less cost [31]. The element dimensions in the clad should also be the same in each direction because the clad is the region of interest. Meanwhile, the element dimensions in substrate adopt the auto-meshed size because the impact of substrate element dimensions is very limited.

The linear element or first-order element is used to avoid potential spurious oscillation when rapid temperature changes are present. The nonlinear element or second-order element can provide higher accuracy when severe element distortion is involved and are suitable for bending-dominated problems. For the same reason, since the clad surface is assumed to be smooth in the simulation, the non-linear element is not necessary. Besides, the linear element is computationally cheaper than the nonlinear element.

Generally, the simulation accuracy has an inverse correlation relationship with the mesh size. To ensure simulation accuracy, the mesh size should be small enough to avoid error accumulation.

On the other hand, small mesh size can cause an excessive number of nodes or elements, which has a positive correlation with the computational cost. Similar to the increment time, mesh size should be designed to balance efficiency and accuracy.

Because the laser energy inside the laser spot is determined by the laser energy received by each node, there should be at least two nodes on the side and center respectively to ensure the minimum accuracy. If there are fewer than 4 nodes in the laser spot, the laser energy distribution is very skewed to the nodal location, which causes the laser energy inconsistency.

Additionally, since the nodal coordinate is necessary to keep track of the nodal activation status, the clad dimension should be evenly divided by the mesh size for calculation convenience. According to equation (3) and (4), the clad height is 0.723 mm and clad width is 2.93 mm, which round to 0.7mm and 3.0 mm respectively, given the initial laser power is 1.0 kW, the feed rate is 1 m/min, the powder flow rate is 23.5 g/min, the laser radius is 1.541 mm.

To summarize, the following factors should be considered when choosing the mesh size:

- At least 4 nodes in the laser spot at any increment.
- The clad dimension should be evenly divided by mesh size.
- Mesh size should be large enough to avoid the excessive computational cost.
- Clad height and width are 0.7 mm and 3.0 mm respectively.

Based on the factors above, the mesh size of clad in the vertical and horizontal direction is 0.7 mm and 1.0 mm respectively. Since the mesh size is determined, the minimum increment time is 0.0048 s according to equation (11). In addition, every node should be inside the laser spot at least for one increment to ensure accuracy except the corner nodes due to the nature of nodal location. Thus, the time increment should not be larger than 0.1 s, otherwise, the side nodes could be skipped

because the two consecutive laser spots are distanced. The figure below shows the laser spot distance when time increment is 0.1 s.

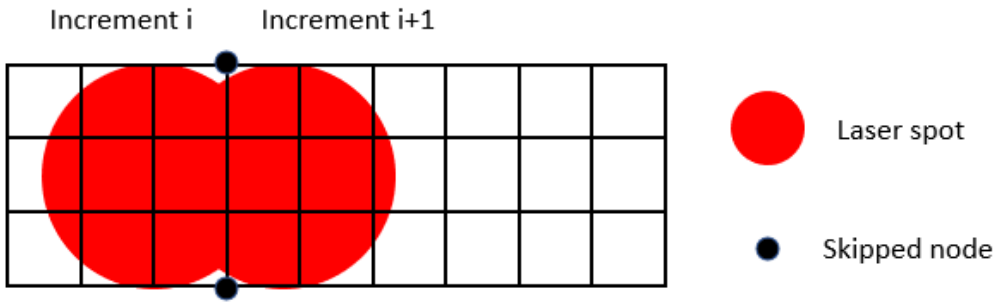

Figure 5. The skipped nodes when time increment is 0.1 second

Based on the reasons above, the time increment is 0.05 s.

2.2 Major Components of DED Modeling

2.2.1 Laser Energy

There are two types of external energy sources in ABAQUS, surface heat flux and body heat flux. Surface heat flux is applied on the surface, and only the nodes within the surface can receive surface heat flux. Body heat flux is applied to a three-dimensional region, and all the nodes within the 3-d region can receive the body heat flux. Considering the laser power penetration depth is generally at 10e-6 m level [32], the laser power is mostly absorbed by the powder on the surface. Thus, the laser power is modeled as surface heat flux.

The laser power distribution has a top hat shape because of the laser diode stacking. The laser power distribution is also shown in the figure below:

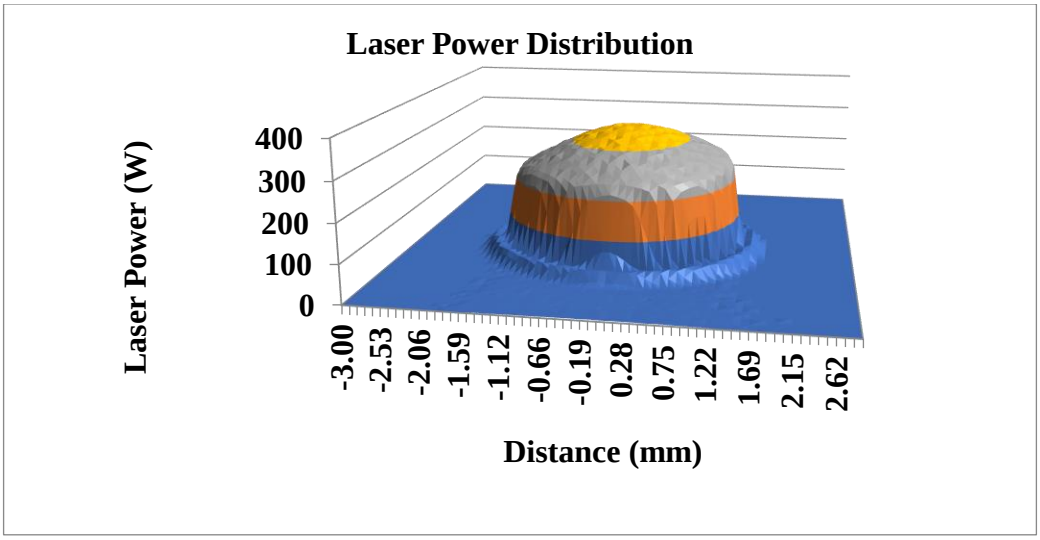

Figure 6. Laser power distribution of the stacked diode laser in the LaserTec 65 DED Hybrid

The laser power is partly absorbed by the powder stream before fused into the melt pool, therefore, the attenuation rate should be considered. The attenuation rate, A_t , was modeled using the theory proposed by [32][33],

$$A_t = (1 - \frac{q_a}{q_l}) \frac{3\dot{m}}{\pi D_p r_p v_p \rho sin\theta} \tag{12}$$

Where q_a is the attenuated laser power, q_l is the incident laser power, $\dot{m}$ is the powder mass flow rate, D_p is the diameter of the powder flow, r_p is the radius of the powder particles, v_p is the powder particle velocity, ρ is the powder density, θ is the inclination angle relative to the surface normal. Other than attenuation, the laser absorption rate of material, α, is estimated by Wirth, et al [34]. By combining the laser attenuation rate and absorption rate, the actual energy transferred from laser power to clad can be written as:

$$\dot{q}_s = \dot{q}_l \alpha (1 - A_t) \tag{13}$$

The magnitude of laser power can be defined by finding the distance between the laser spot center and the current node coordinate. If the nodes are within the 1.541 mm of the laser spot, the laser power can be calculated by the laser power distribution equation (13), otherwise, the power is 0.

$$\dot{q}_s = -17916r^6 - 12476r^5 + 29465r^4 + 16712r^3 - 61689r^2 - 9069.4r + 334480 \quad (14)$$

Where r is the distance from laser spot center to nodal location.

2.2.2 Material

The material used in this study is stainless steel 316L. The conduction coefficient and specific heat are referenced from the book written by Mills [35]. In this book, the temperature-dependent conduction coefficient and specific heat values are provided with approximately 100 °C increment. Additionally, the latent heat is evenly distributed ranging from the solidus temperature 1385 °C to liquidus temperature 1450 °C and coded into the DFLUX subroutine. Moreover, study also shows the conductivity of the melted metal is enhanced due to the Marangoni effect [36]. The conduction coefficient is modeled with increasing by 4 times if the temperature is above the liquidus temperature. The density of the material is also temperature-dependent due to the thermal expansion effect. However, the thermal expansion is not considered in this study and the density variance between room temperature and liquidus temperature is less than 9%, therefore, the density is fixed in the simulation with 7950 kg/m^3.

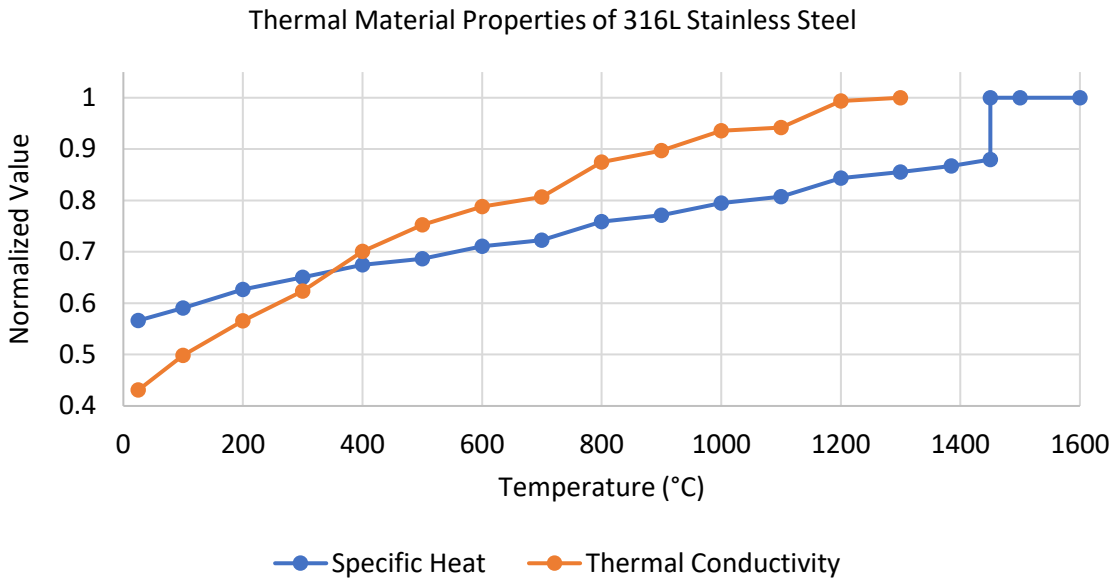

Figure 7. Conductivity and specific heat of stainless steel 316L

2.2.3 Film condition

Considering the energy lost by radiation is very limited, especially with small temperature values, the computational cost is unnecessarily high compared with convection. By following the method of Lindgren [37], the conduction coefficient and radiation coefficient are combined to improve the calculation speed. The combined coefficient can be calculated as the equation below:

$$h = (6E^{-5}T + 0.0121) \quad (15)$$

The environmental temperature of the model is constant at 25 °C except for the bottom surface because the air temperature is increased by 4 °C due to the heating from the part and fixture [38].

2.3 Thin-wall simulation

The relationship among clad size, cladding parameters, and steady-state temperature is firstly investigated on a simple clad shape, thin wall. A 25 mm thin wall model is created to highlight the difference between ~~without control method and with control method~~a controlled and an

uncontrolled deposition. Because the melt pool energy is strongly influenced by the accumulated heat in the clad, the input energy needs to be balanced with the accumulated energy to avoid deformation due to excessive melt pool energy. Thus, instead of keeping track of the melt pool size and temperature distribution in real-time, the internal energy of the melt pool is the control target in thin wall simulation.

Because the accumulated heat is essentially the clad surface temperature, the correlation between cladding parameters and steady-state temperature is also revealed in the melt pool energy control simulation.

2.3.1 Thin Wall Model Build

The thin wall model is composed of the substrate and thin wall shape clad, shown in figure 8, whose dimensions are listed in table 3.

Table 3. The 25 mm thin wall model dimensions

	Height (mm)	Width (mm)	Length (mm)
Clad	22.4	3	25
Substrate	25	30	50

The thin wall has 32 layers in total, and each layer height is pre-determined to be 0.7 mm. The mesh size choosing principle is already explained in section 2.1.2 and the values are listed in table 4.

Table 4. The 25 mm thin wall mesh size

Mesh size	Height (mm)	Width (mm)	Length (mm)
Clad	0.35	0.25	0.25
Substrate	5	5	5

It should be noted that the mesh size of the thin wall is initially 0.25 mm instead of 1mm because the thin wall dimensions are relatively small and will not cause an excessive number of elements

for using a fine mesh. After meshing, the model contains 76800 clad elements and 136224 elements in total.

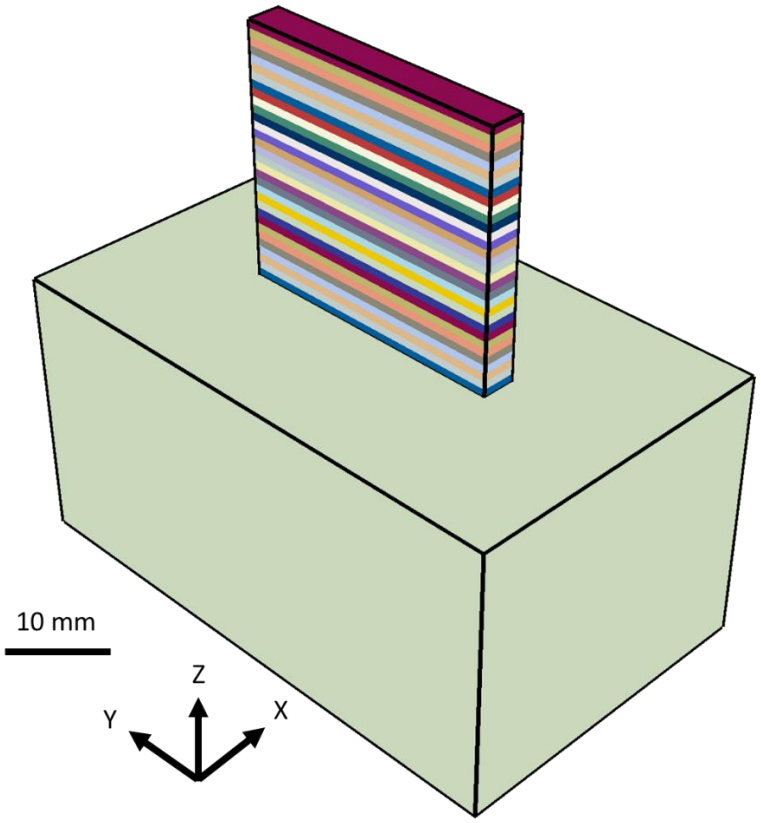

Figure 8. Thin wall model in isometric view

The thin wall material is 316L, whose property is explained in section 2.2.2 and initial values are shown in table 5.

Table 5. The initial values of material properties of substrate and clad

Material Property	Conductivity W/(m·K)	Specific Heat kJ/(kg·K)	Film Coefficient W/($m^2 \cdot K$)	Active Boolean
Substrate	13.4	0.47	0.0121	1
Clad	0.001	0.47	0.0121	0

Other than the physical material property, a new property, active, is introduced to help control the clad geometry during simulation. The active is a Boolean property that determines whether the

node or element is included in the clad. Inactive nodes are assigned with 0 and have nearly zero conductivity, 0.001 W/(m·K), compared with the conductivity at room temperature, 13.4 W/(m·K). The low conductivity ensures the nodes inside the inactive element cannot receive any heat transferred from the nearby active nodes. An inactive node is activated if its nodal temperature is greater than liquidus temperature, 1450 ℃, and assigned with 1. Once a node is activated, the node is active in the rest of the simulation and has regular conductivity. Active element is defined as the element which contains at least 6 active nodes. The inactive nodes inside an active element cannot conduct heat with each other but can receive heat from the connected active node in the same element. For inactive elements, there is no heat conduction for all the nodes inside no matter active or not, which is presented in figure 9. It should be noted that all the substrate nodes are initially active and all the nodes solely belonging to clad are inactive. The substrate and clad interface nodes are also initially active.

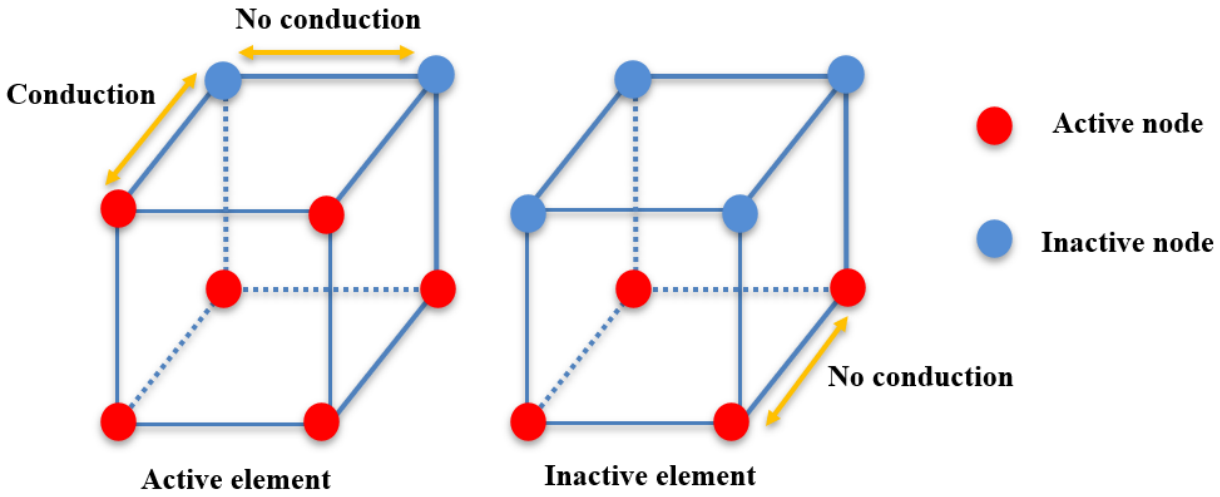

Figure 9. The heat transfer of active nodes and inactive nodes

The heat dissipation of the clad nodes depends on the nodal location. The side surface nodes always have convective heat transfer with the environment no matter active or not. The heat dissipation

of the internal nodes only happens when the internal nodes are active and located at the current clad top surface. Because the clad shape varies with elements adding to the clad every increment, the clad top surface is tracked by the vertical coordinates of the active nodes in both FILM subroutine and UMATHT subroutine to ensure heat dissipation takes place in the correct location. Figure 10 shows the heat dissipation on clad top surface in front view by assuming two nodes are added in the clad in one increment.

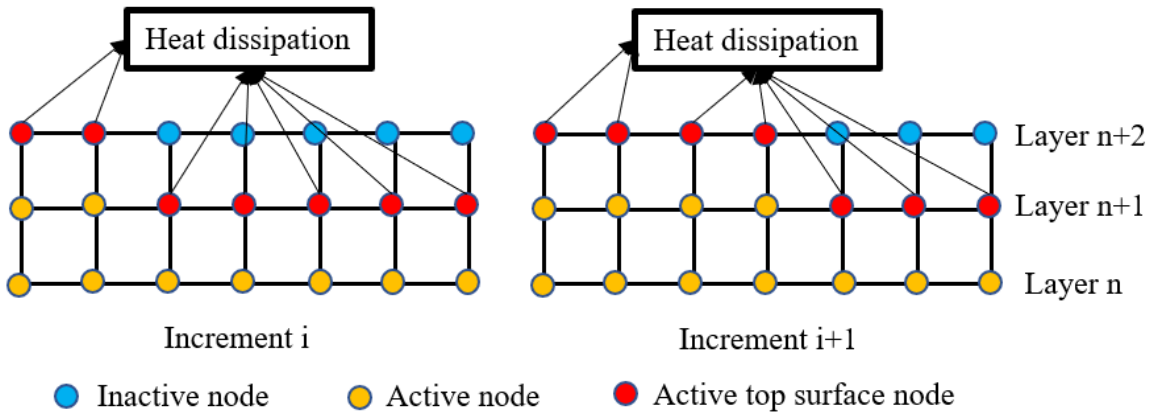

Figure 10. The heat dissipation on clad top surface in front view

Unlike heat dissipation, the interaction between nodes and laser is not always happened on the clad top surface nodes. The laser power and powder are applied on the clad top surface simultaneously in the actual cladding process, which is simulated as the laser power is initially applied on the clad top surface nodes and activating the nodes through time. After the clad surface nodes are heated over the liquidus temperature 1450 ℃, the laser power moves to the node above the current node. This process is repeated until the newly added layer height is equal to the pre-determined layer height, which is presented in figure 11.

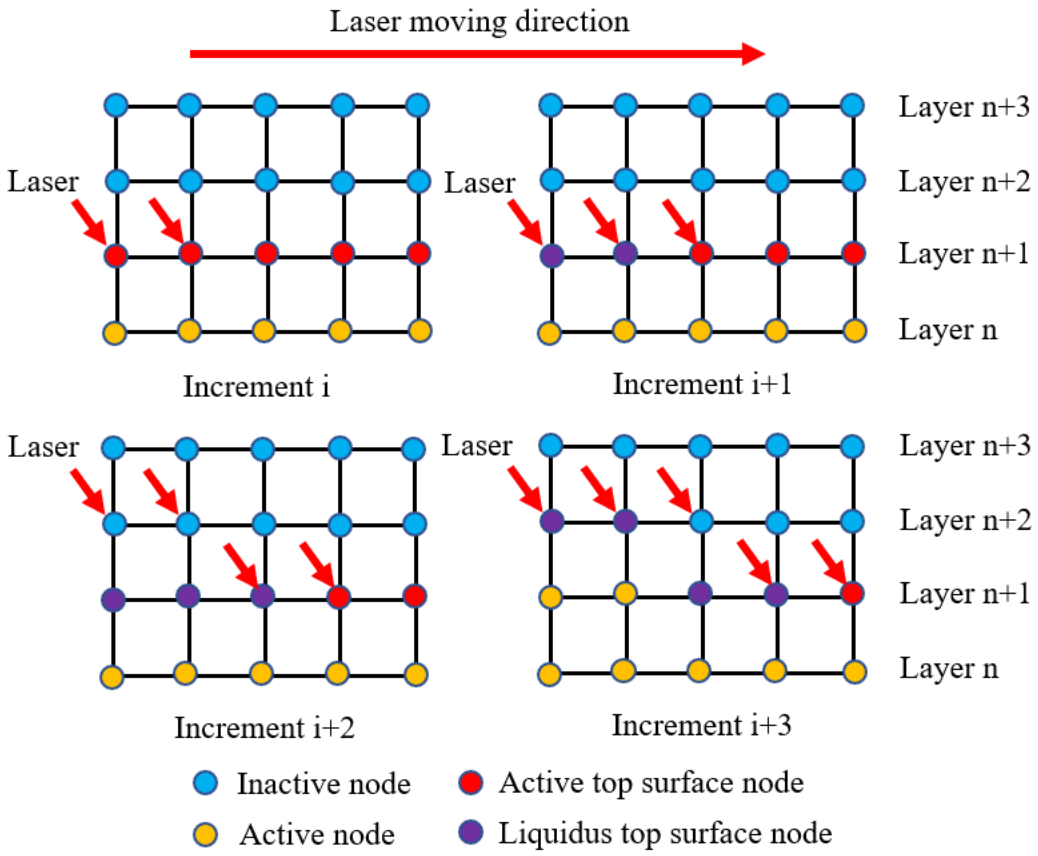

Figure 11. Interaction between laser and node

2.3.2 Thin wall laser track

The laser spot track of the thin wall initially moves in the positive x-direction and reverses the direction after one layer is finished. The clad is built by repeating moving back and forth patterns, which is also known as a zig-zag laser track. ~~Because the laser head needs approximately 1 s to speed up from 0 to stabilized feed rate and cladding should be conducted with stabilized feed rate, the initial position of the laser head is 1 s traveling distance away from the clad edge, showed in figure 12.~~ An acceleration offset distance is programmed into the path to allow the tool to reach the target cladding feed rate, which takes 1 s. For the same reason, the end position of each layer is also 1 s traveling distance away from the other side of the clad. Thus, the interlayer time is 2 s by assuming the feed rate of the next layer is about the same.

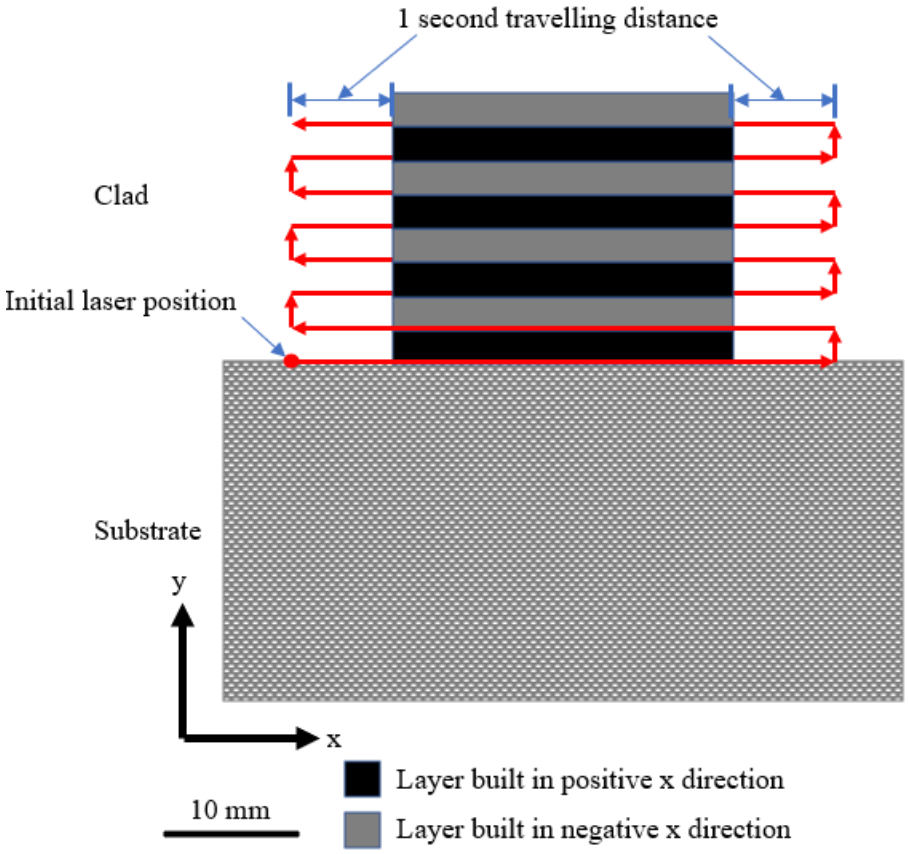

Figure 12. The laser track schematic with exaggerated layer height

It should be noted that the laser is off when the laser spot center is away from the clad, but powder flow is on in the entire cladding process. Additionally, the travel distance away from the clad depends on the feed rate of the current layer and next layer, thus, the travel distances away from clad of two consecutive layers are not necessarily the same with feed rate control. The vertical travel time is ignored because the distance is relatively small compared with horizontal travel time.

2.3.3 Thin wall simulation with constant cladding parameters

The thin wall is severely deformed with recommended cladding parameters as mentioned in section 1.2. The simulation with static cladding parameters, listed in table 6, is conducted to set a comparison baseline for the simulations with the control method.

Table 6. Recommended static cladding parameters

Recommended/static cladding parameters	
Laser power	1.7 kW
Feed rate	1m/min
Powder flow rate	23.5g/min

The clad width and melt pool energy of the constant cladding parameter simulation is showed in figure 13.

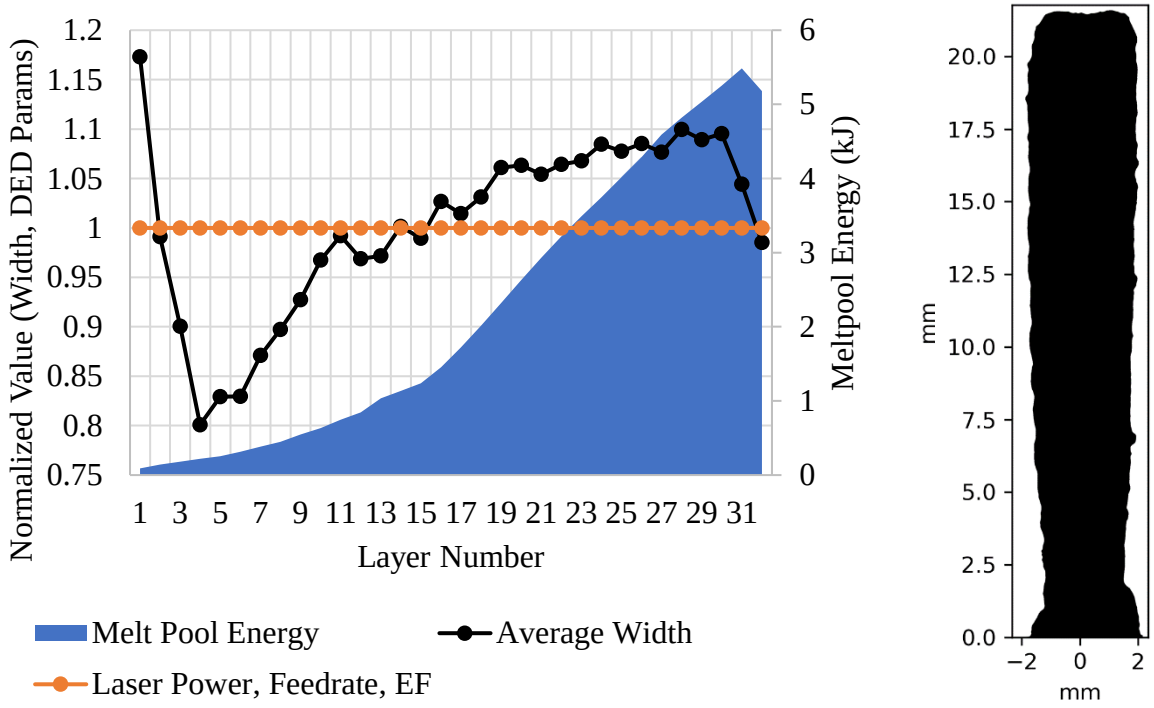

a) b)

Figure 13. a) The melt pool energy and clad width built by constant cladding parameters, and b) the clad width image taken by Micro-Vu

It is apparent from figure 13 that thin wall width is increasing with the melt pool energy except for the top layers due to the nature of the round shape on top of the clad. The average clad width is 3.24 mm while the laser spot diameter is 3.14 mm. The melt pool energy curve of the last 21 layers is steeper than the first 11 layers, but the clad width curve of the last 21 layers is flatter than the

first 11 layers. The curvature difference indicates the clad width is sensitive to the melt pool energy increase before the melt pool is too intense. The peak melt pool energy has a nearly linear relationship with the layer number. To maintain geometry consistency, the melt pool energy needs to be controlled by reducing the energy flux into the melt pool. The energy flux can be reduced by either reducing the laser power or increasing the feed rate according to equation 1.

2.3.3 Thin wall simulation with laser power-based control

As discussed in section 2.1, since the thin wall is severely deformed due to energy accumulation, laser power is usually manipulated as the only control variable to maintain the melt pool energy distribution consistency. The melt pool energy distribution is defined as the melt pool internal energy through the cladding time of each layer. If the cladding process is approaching steady state, the melt pool energy distribution should have relatively little variance. Therefore, as the control target, the melt pool energy distribution is checked at the end of each layer and compared with the target melt pool energy distribution to see if the cladding process is at a steady state.

However, it is ineffective to directly calculate the error of two sets of melt pool energy data for two reasons. The first reason is that the melt pool energy is not evenly distributed along the cladding time, thus, the difference between each increment and their corresponding increment also widely varies. The second reason is that the number of increments of two consecutive layers is not necessarily the same because of the feed rate difference. The melt pool energy of certain increment in the current layer may not have a corresponding increment in the previous layer. Therefore, the melt pool energy distribution comparison is characterized as the peak melt pool energy comparison and data set similarity. Peak melt pool energy is the maximum melt pool energy of a layer, which is generally located in the middle of the clad. Melt pool energy distribution similarity is calculated by cosine similarity method, presented in equation 16.

$$s_C = s_C(d_1, d_2) = \frac{\boldsymbol{d}_1 \boldsymbol{d}_2}{|\boldsymbol{d}_1| \cdot |\boldsymbol{d}_2|} = \frac{\sum_{i=1}^{n} d_{1i} d_{2i}}{\sqrt{\sum_{i=1}^{n} d_{1i}^2} \sqrt{\sum_{i=1}^{n} d_{1i}^2}} \quad (16)$$

Where s_C is the cosine similarity; d_1 is the melt pool energy distribution of the current layer; d_2 is the melt pool energy distribution of the previous layer. The cosine similarity treats the two data sets as vectors and describes how the similarity of the vectors in terms of distribution. If vectors distributions are the same, the equation will return 1. According to equation 16, the vectors should have the same length. If the vectors' length is different, the shorter vector will be filled with zeros depending on the vector length difference. Nevertheless, the magnitude difference between two vectors is not considered in the cosine similarity method, which is why the peak of the melt pool energy needs to be compared. If peak melt pool energy difference is small enough and cosine similarity is close to 1, the cladding process is considered at a steady state.

The layer-wise control is based on the knowledge of the cladding condition. To better learn the cladding condition, a series of simulations are conducted with various substrate temperatures to create a look-up table. A 10-layer sub-model of the thin wall is created to lower the computational cost for the look-up table, figure 14. The model dimension is listed in table 7.

Table 7. The sub-model dimensions

Dimension	Height (mm)	Width (mm)	Length (mm)
Clad	7	3	50
Substrate	25	30	100

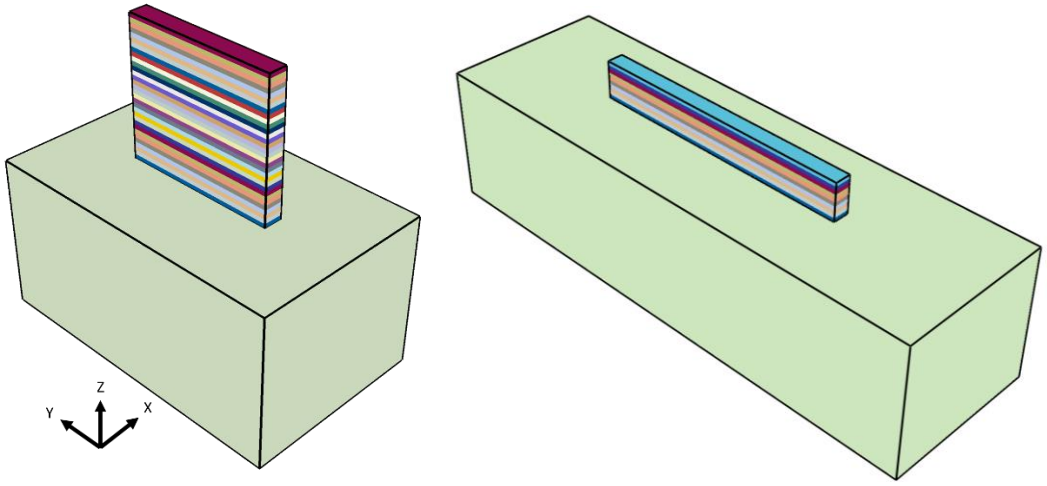

a) b)

Figure 14. a) 32-layer thin wall model; b) 10-layer thin wall sub-model

According to the previous simulations, the temperature distribution of the layers located at 5 layers below the current cladding layer has very little impact on the melt pool energy distribution of the current layer as long as the temperature gradient in the vertical direction is approximately the same. Thus, the sub-model consists of 8 initialized layers and 1 cladding layer to ensure accuracy. The look-up table data is extracted from the finished 9^{th} layer. The data extraction follows the principle below:

1. The data is collected at 1.0 s after the 9^{th} layer is done for 0.5 s to avoid inconsistent increment time, which is usually 3 increments. The latest value is used for the look-up table.
2. The surface temperature and melt pool energy are sorted at the end of the layer in the subroutine. The nodes whose temperature is less than 30 ℃ are not counted for better accuracy.
3. The peak melt pool energy is using the average value of the 3 largest values of the layer.

Temperature initialization of the first 8 layers of the sub-model was done by transferring simplified results from the 32-layer thin wall model with no melt pool energy control. The laser is applied on the 9th layer after the simulation started for 0.5 s. Then the sub-model is applied with different sets of laser power and feed rate to produce different outcomes. Because the thin wall length of the sub-model is 50 mm instead of 25 mm, the peak melt pool energy of the sub-model is generally slightly larger than the 25 mm with the same initial temperature distribution, especially when the initial temperature is high.

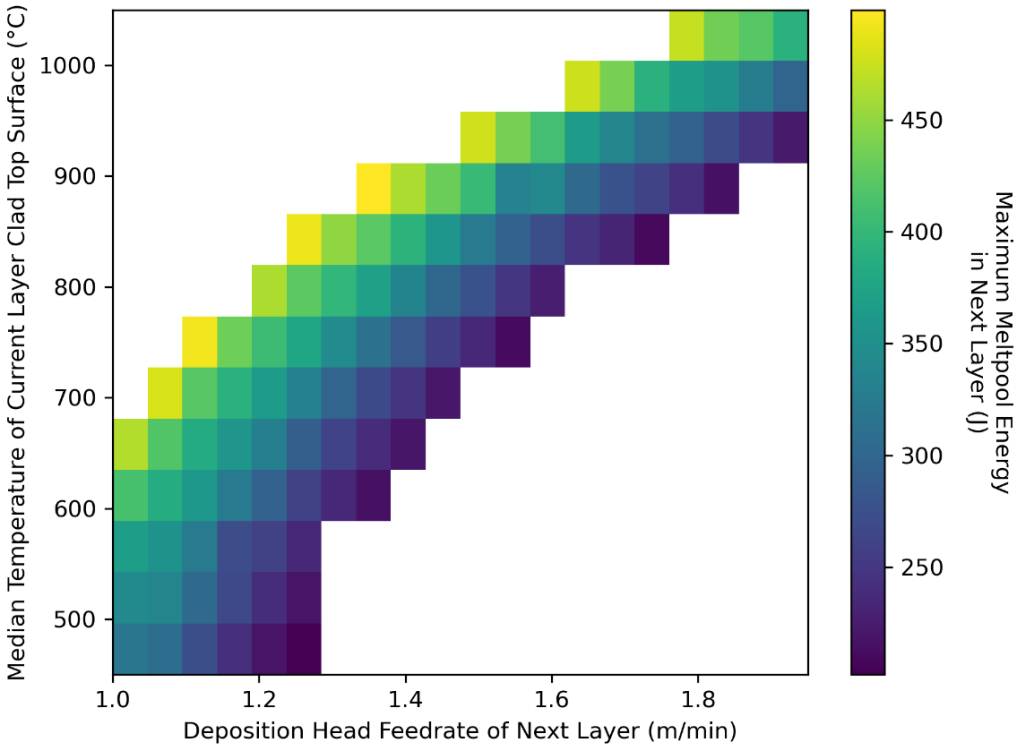

a)

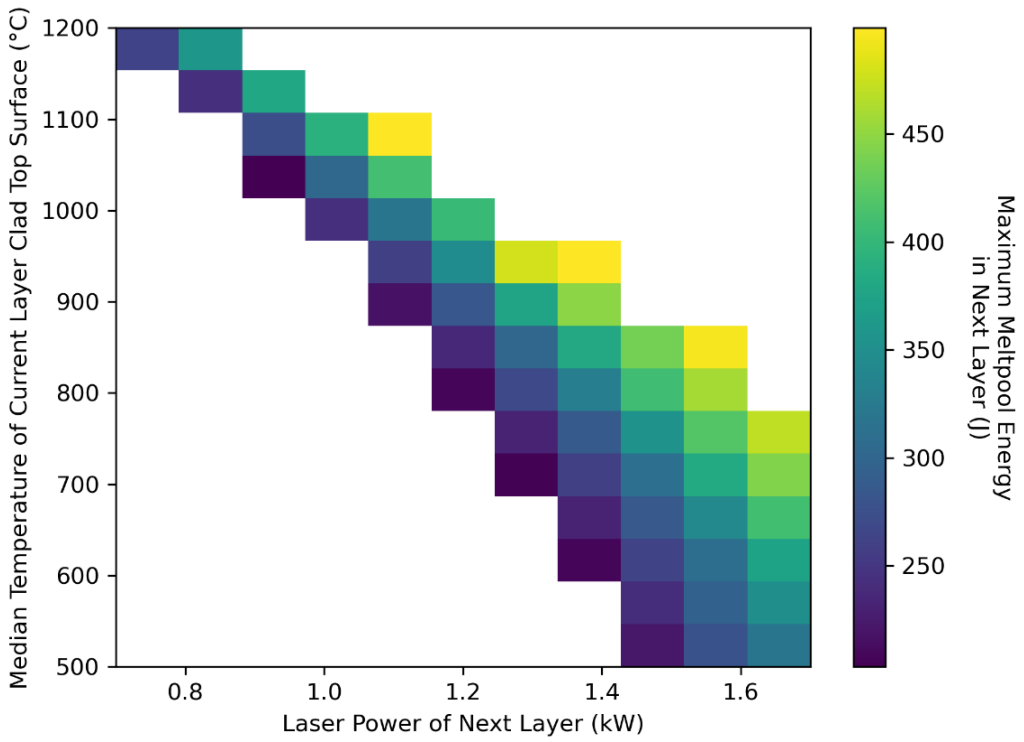

b)

Figure 15. a) Response surface of feed rate on melt pool energy and b) response surface of laser power on melt pool energy

The laser power range of the look-up table, figure 15, is from 0.7 kW to 1.7 kW. If out of this range, the laser power is either insufficient or unnecessary. The feed rate range is from 1 m/min to 1.8 m/min. The upper bound of feed rate is limited by powder flow rate if the layer height is fixed at 0.7 mm by equation 4.

According to the simulation with no control, the melt pool energy is about 350 J when the clad width is approximately 3 mm. Therefore, the control target is to maintain the melt pool energy at 350 J. At the end of each layer, the look-up table is invoked to calculate the next layer's laser power by linear interpolation.

The initial cladding parameters are the same as recommended cladding parameters, table 6. Except the laser power is adjusted every layer, the cladding process is the same with cladding with no control. The simulation result is shown in figure 16.

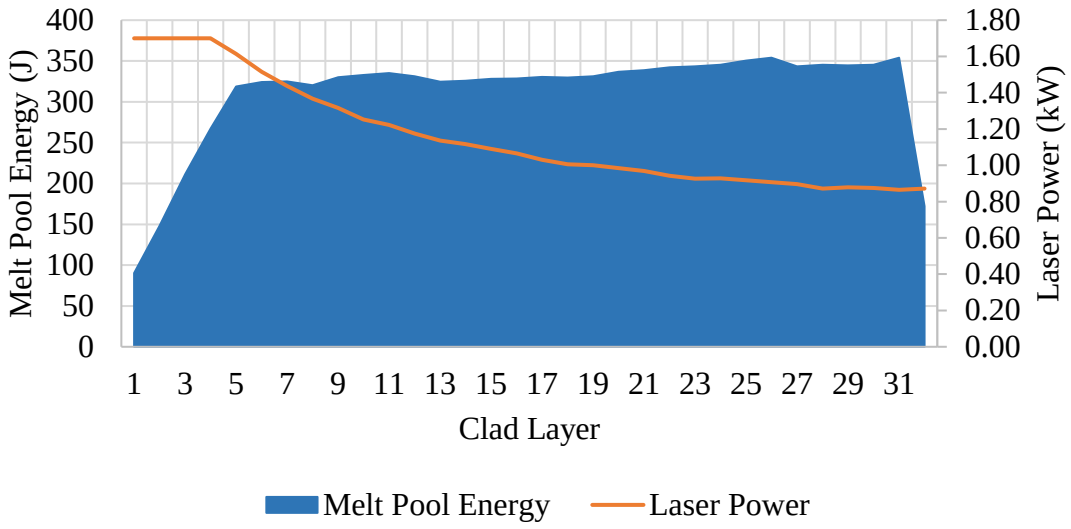

Figure 16. Simulation result of laser power-based control

From the figure above, after 27 layers, both laser power and melt pool energy are gradually stabilized. It can be noticed that the melt pool energy is slightly lower than 350 J for most of the layers. The potential error sources are:

- The peak melt pool energy of the 50 mm sub-model is higher than 25 mm thin wall model. The laser power obtained from the look-up table is suitable for 50 mm thin wall but a little insufficient for 25 mm thin wall, which is the major reason for insufficient melt pool energy.
- The relationship between melt pool energy and laser power is non-linear, but the laser power is calculated by linear interpolation.

- The initial temperature of the sub-model uses the nearest value from the no-control simulation, the temperature gradient of the sub-model in the vertical direction can be slightly off.

The average error is 14 J from layer 5 to layer 32, roughly 4% off the control objective. The first 4 layers are included because the laser power of the first 4 layers is 1.7 kW due to the upper bound of the look-up table.

2.3.4 Thin wall simulation with feed rate control

Similarly, with the laser power control, the look-up table in figure 16 is used to select the feed rate for the next layer. The feed rate is calculated by the linear interpolation at the end of each layer in DLFUX subroutine. The control objective is the same as the laser power control, maintaining the melt pool energy at 350 J. The simulation result is shown below, figure 17.

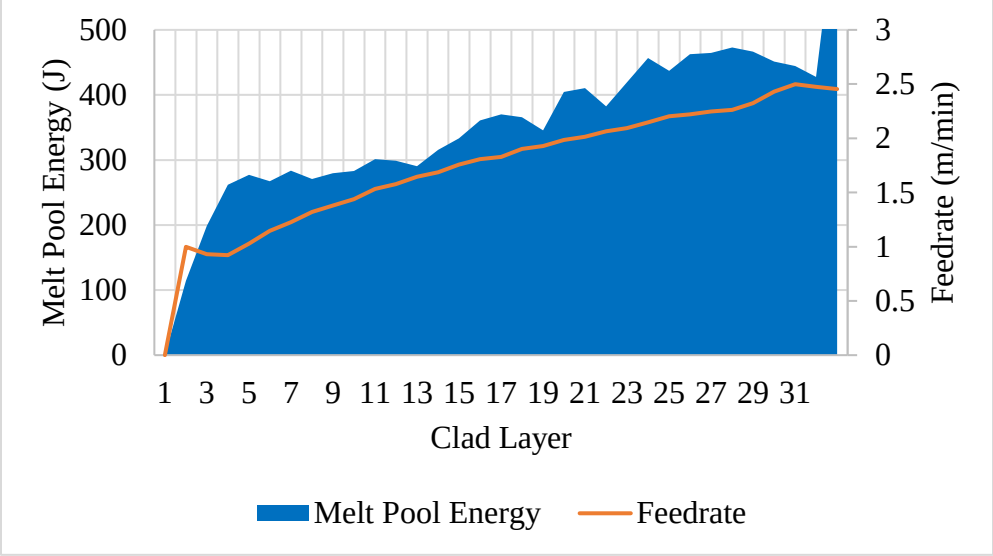

Figure 17. Simulation result of feed rate-based control

The error of feed rate-based control method, 67 J, is approximately 19% off the control objective and much larger than laser power control. Most of the error is from the difference between the

peak melt pool energy of the sub-model and the peak melt pool energy of the 25 mm thin wall. This difference is especially significant when the feed rate is close to 1 m/min, which is the major reason for the insufficient melt pool energy in the early layers. Because of the large error in early layers, the melt pool energy oscillation of the feed rate control is much larger than the oscillation of laser power control. Even though the feed rate control is less effective than the laser power control in terms of stability, the overall fabrication time, 93.7 s, is reduced by 22% by feed rate-based control. Considering the interlayer non-cladding time, 48 s, is 68% of the overall fabrication time, the actual cladding time is reduced by 38%.

The feed rate control effectiveness can also be evaluated from the perspective of clad top surface median temperature. The median temperature is collected 1.5 s after the current layer is finished to keep consistent with the data collecting time of previous simulations. Like the melt pool energy distribution, the median temperature is another indication of the cladding process approaching stability, figure 18.

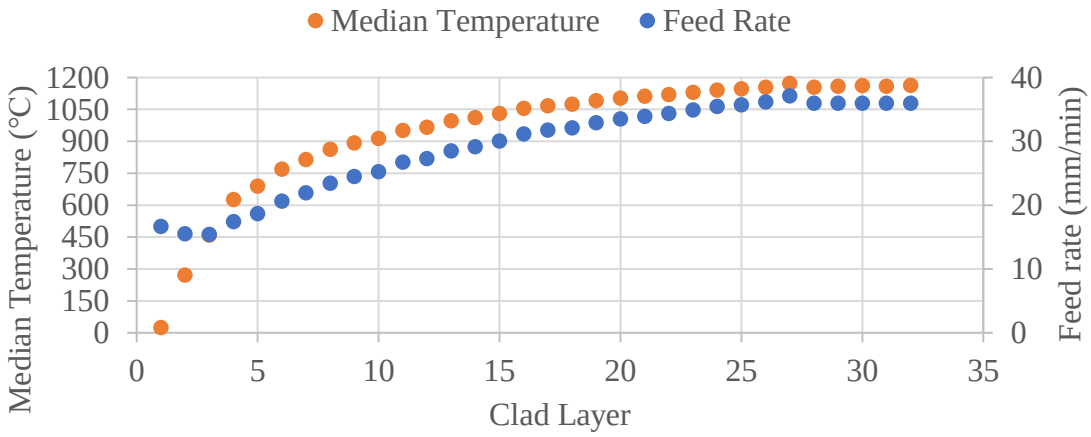

Figure 18. Clad top surface median temperature in feed rate-based control simulation

2.4 Square Block Simulation

To test the control method on more general shapes, the square block model is built with the same material as thin wall model. The square model is a closed-curve shapes and has the distinct advantages of being easy-to-mesh and having explicit nodal coordinates, which are important in the simulation. A series of square blocks are tested with laser power control and feed rate control to find the suitable control method for a given dimension.

2.4.1 Block model build

The square block model is composed of the substrate and square block clad, figure 19. The square block is hollow inside and consists of 4 identical thin walls. The control method is firstly tested on a 25 mm square block. The dimensions are listed in table 8.

Table 8. The square block model dimensions

	Height (mm)	Width (mm)	Length (mm)
Clad	28	3	25
Substrate	25	50	50

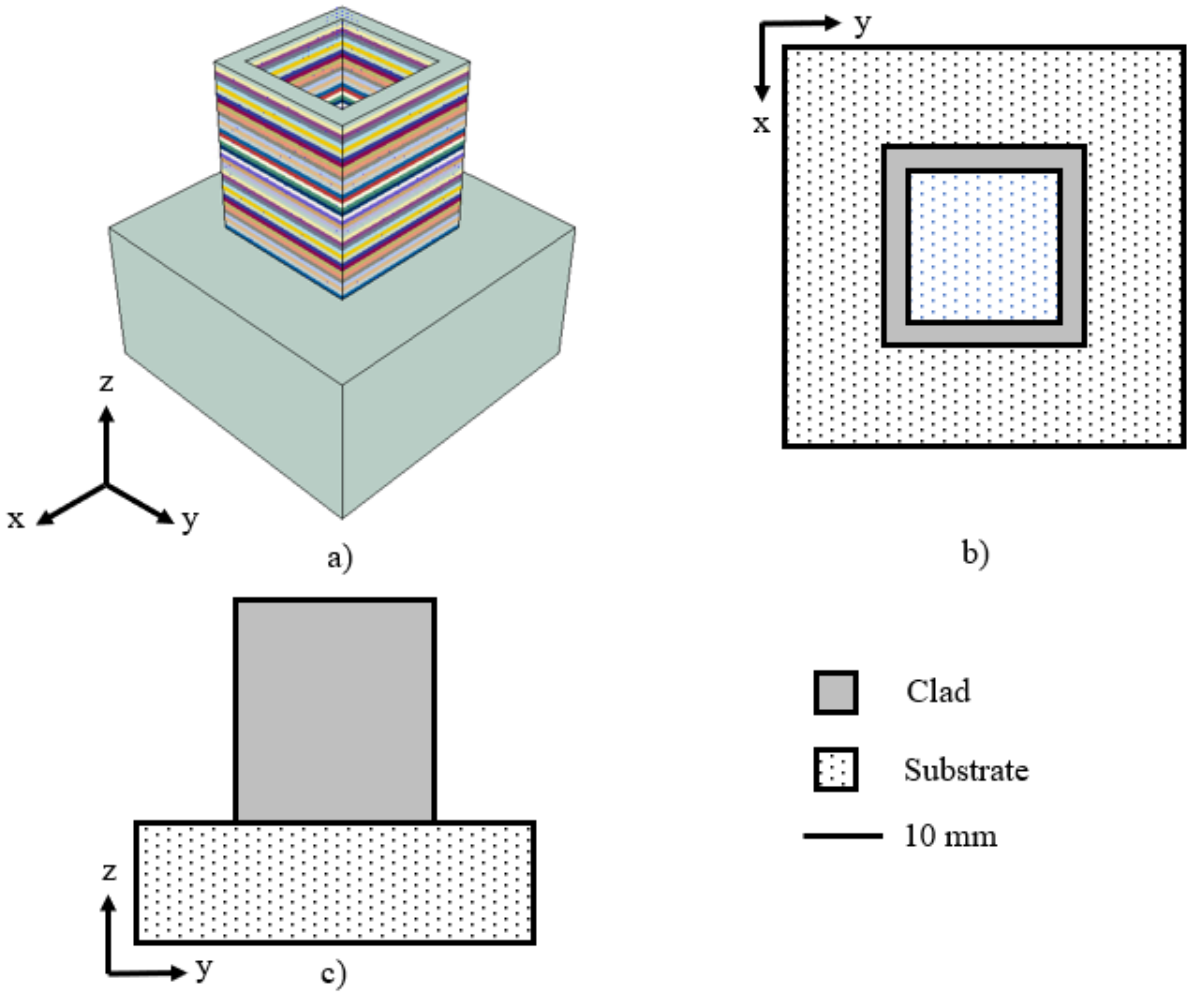

Figure 19. a) 40-layers square block in isometric view; b) top view; c) front view

The square block has 40 layers in total, and each layer height is also 0.7 mm to keep consistent with the thin wall. Because the square block model size is much larger than thin wall, the mesh size, table 9, is increased to reduce computational cost caused by excessive elements.

Table 9. The thin wall mesh size

Mesh size	Height (mm)	Width (mm)	Length (mm)
Clad	0.7	0.5	0.5
Substrate	5	5	5

The model contains 42240 elements in clad and 93984 elements in total after meshing.

2.4.2 Square Block Laser Track

Clockwise laser track is used in the square block model, figure 20. The interlayer time is ignored in simulation because it is only used to lift the laser head for 0.7 mm, approximately 0.042 s.

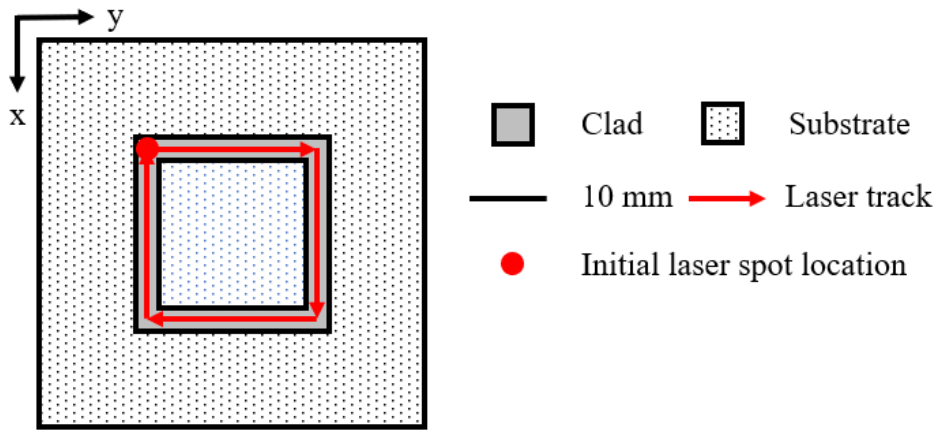

Figure 20. Laser track of the square block model from top view

2.4.3 Temperature control with fuzzy controller

Similar to the knowledge-based controller in thin wall simulation, a fuzzy controller is developed in square block simulation to improve the cladding efficiency and accuracy by manipulating the laser power and feed rate. Both laser power control and feed rate control using fuzzy logic are tested and compared with simulation results with no control. Additionally, instead of controlling the melt pool energy, the top surface median temperature of the clad is the control target.

Compared with the conventional control method, the fuzzy control does not require the explicit math model of the cladding process, which is highly non-linear and hard to obtain. The fuzzy controller takes two inputs, the clad top surface median temperature difference between two consecutive layers and the temperature difference between the current layer and control objective, and has one output, the laser power of the next layer.

$$de = T_{previous} - T_{current} \tag{17}$$

$$error = T_{objective} - T_{current} \tag{18}$$

Where $T_{current}$ is the current clad top surface median temperature, $T_{previous}$ is the median temperature of the previous layer, $T_{objective}$ is the objective temperature, de is the median temperature difference, dl indicates the temperature difference is based on layer, de is also written as de/dl to differentiate from the time-based controller.

The fuzzy controller follows the if-then linguistic rule. The linguistic value 'small' and 'large' are used to describe the error and de/dl. To differentiate the positive value and negative value, 'positive large' is abbreviated to 'PL', and 'negative large' is 'NL'. Compared with the classic logic which takes discrete inputs, either 1 or 0, the fuzzy logic inputs are evaluated continuously between 1 and 0 under the linguistic rules. The information processing of fuzzy controller can be summarized as:

1. Fuzzification: Use appropriate membership functions to convert discrete values into a certain degree of linguistic values.
2. Inference: The fuzzy values are processed by the control rule to generate a result for each rule.
3. Defuzzification: The results are combined by the control rule and converted back to the discrete value as output.

Since the controller is used to maintain the temperature distribution instead of the temperature, the plant in fuzzy control schematic, figure 21, is the clad formation process.

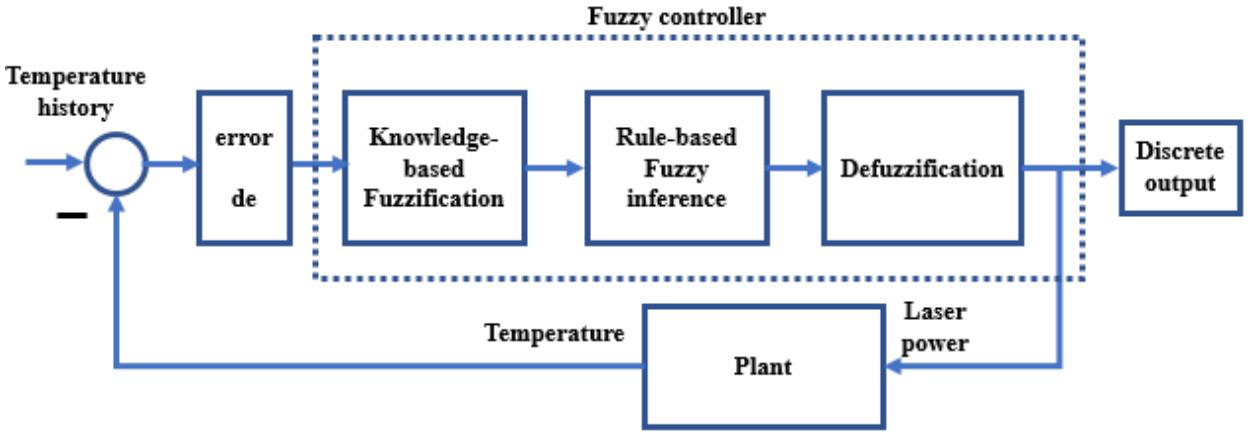

Figure 21. Fuzzy control schematic

The fuzzy set and membership function is determined by the simulation without a control method. From figure 22, it can be concluded that the square block is deformed after 32 layers because the median temperature of the newly added clad is above the liquidus temperature. For the thin wall simulation without control, the clad width is 3 mm when the median temperature is approximately 1200 ℃. Since it takes more time for a 25 mm square block to complete a layer, 5.28 s, than for a 25 mm thin wall, 3.5 s, the cooling time is also longer than thin wall. Therefore, the control objective is set to 1150 ℃ to prevent deformation. 50 ℃ error is defined as ‘large’ in the linguistic rule. The ‘small’ is temporarily defined as half of the large for the sake of simplicity. If the error is 0, it is also defined as ‘zero’ linguistically.

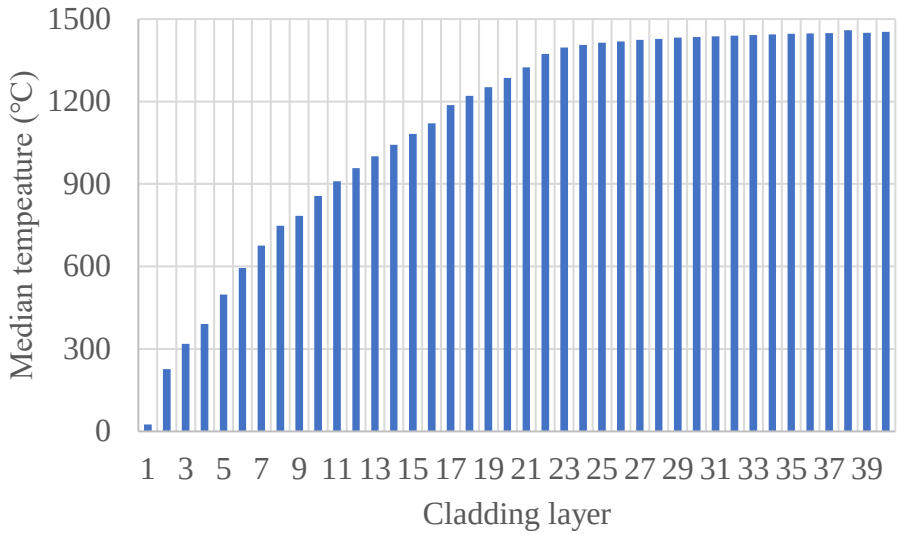

Figure 22. The median temperature of 25 mm square block with no control

Similarly, since the median temperature increment per layer is roughly 50 ℃ when the median temperature is 1200 ℃ without control, any median temperature increment should be deemed as 'large' if the increment is greater than 50 ℃ under control. The 'small' increment is also half of the 'large' increment. The fuzzy set of inputs is summarized in table 10.

Table 10. The fuzzy set of error and de/dl

	Negative large (℃)	Negative small (℃)	Zero (℃)	Positive small (℃)	Positive large (℃)
Error	-50	-25	0	25	50
de/dl	-50	-25	0	25	50

It should be noted that 'negative large' is initially set to -250 ℃ to avoid overshoot. After the error is greater than -50 ℃, the 'negative large' is back to -50 ℃. Thus, the output is adjusted by fuzzy controller when the error is greater than -250 ℃ instead of -50 ℃.

The triangle-shaped membership functions for the fuzzy sets are adopted in this controller and coded into DFLUX subroutine. Each discrete input is converted to a certain degree of linguistic value by the corresponding membership function, figure 23.

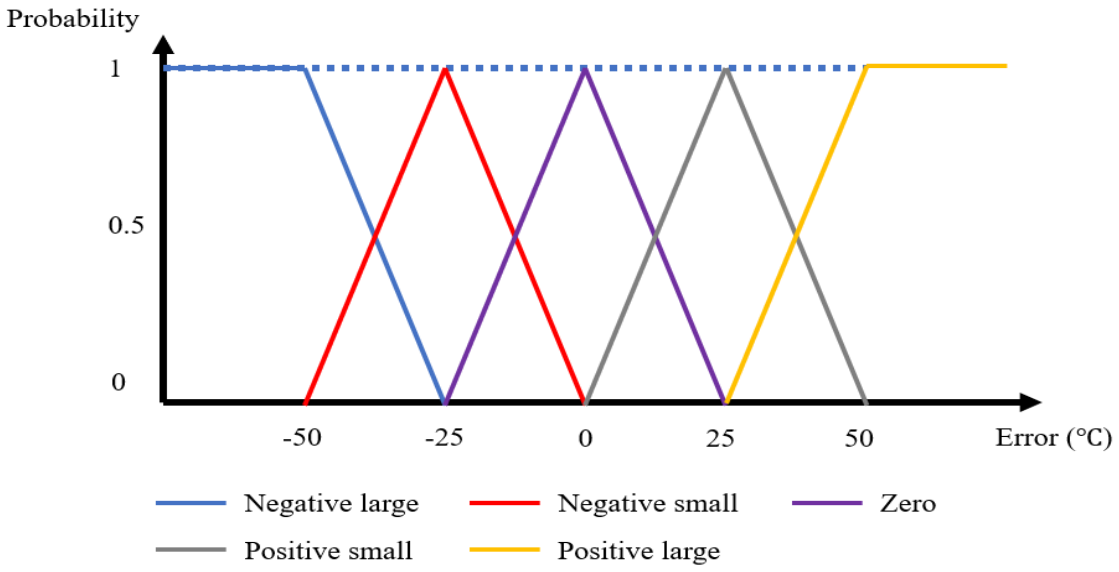

a)

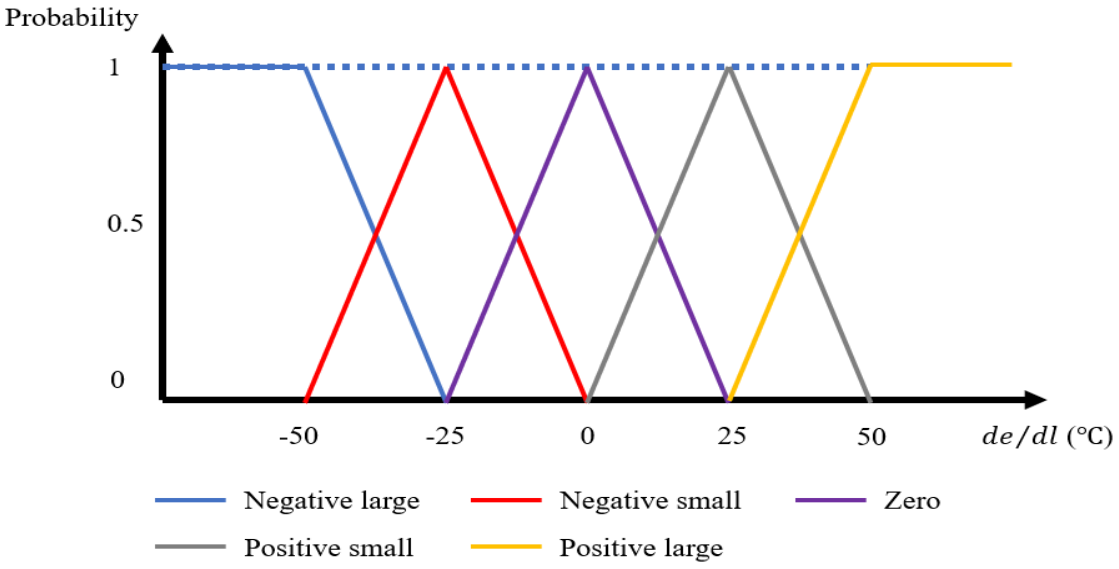

b)

Figure 23. Membership function for a) error and b) de/dl

Once the inputs are fuzzified, the inference rules are invoked to generate the fuzzified output by combining the linguistic values. For instance, if the error is 'positive large', and the de/dl is also 'positive large', then the laser power should be 'very large'. Similarly, if the error is 'zero', and

the de/dl is also 'negative small', then the laser power should be 'small'. Max-Min composition method is used for inference rule combination. In Max-Min inference, the membership functions are combined by fuzzy logic AND operation, equation 18.

$$R_1 \circ R_2 = max\{min[(R_1(error, de/dl), R_2(error, de/dl)]\} \quad (18)$$

Where R_1, R_2 are the two different rules applied in the inference process. The inference rules are listed in table 11.

Table 11. The inference rules of fuzzy controller

	de/dl					
error		NL	NS	Z	PS	PL
	NL	VS	VS	VS	S	M
	NS	VS	VS	S	M	L
	Z	VS	S	M	L	VL
	PS	S	M	L	VL	VL
	PL	M	L	VL	VL	VL

Laser power control with fuzzy logic is tested first. The output of the fuzzified value is laser power increment, which is the laser power difference between the next layer and current layer, equation 19.

$$q_{n+1} = q_n + \Delta q \quad (19)$$

Where q_n, q_{n+1} are the laser power of layer n and layer n+1 respectively, Δq is the laser power increment.

For the layer-wise controller, the control variable is only changed at limited times. Once there is an overshoot in the median temperature, it takes several layers to eliminate the overshoot for the fuzzy controller, which is the potential source of deformation. To avoid overshoot, the 'large' laser power increment is set to 0.1 kW. The 'small' laser power increment is conventionally half of the

'large' laser power increment. The fuzzy set and membership function of laser power increment is shown in table 12 and figure 24.

Table 12. The fuzzy set of laser power increment

	Very small (kJ)	Small (kJ)	Medium (kJ)	Large (kJ)	Very large (kJ)
Δq	-0.1	-0.05	0	0.05	0.1

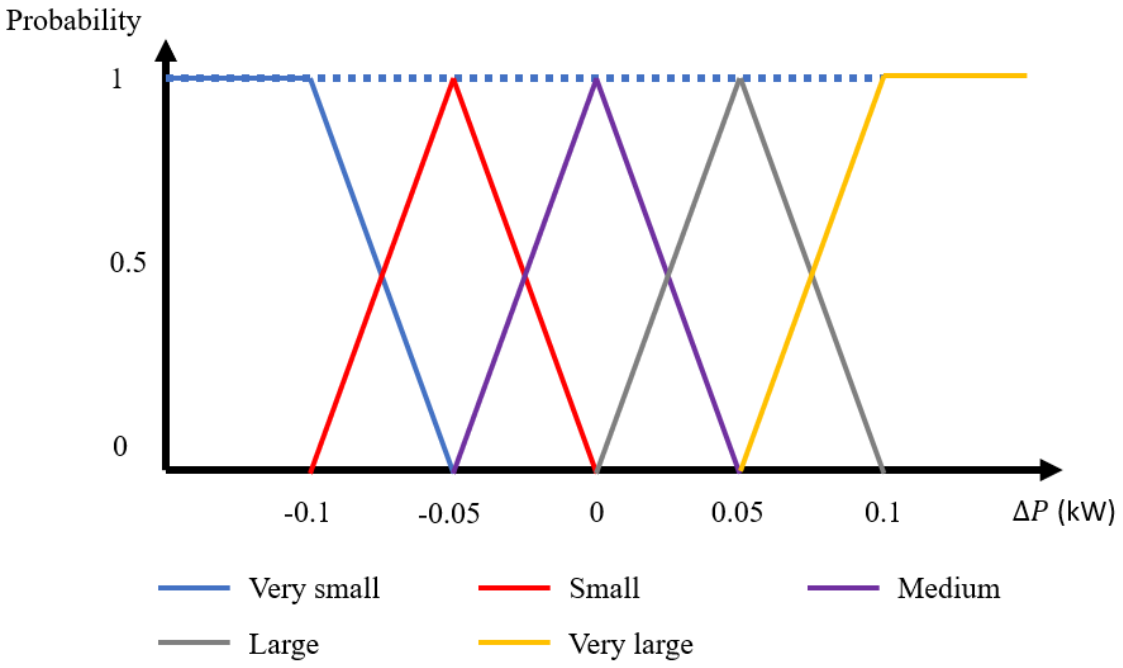

Figure 24. The membership function for laser power increment

After the fuzzified output is converted back to the discrete value in the de-fuzzification component by using the center of gravity method, shown in equation 20, the laser power is used in the next layer.

$$\Delta q_o = \frac{\int \mu(x) \cdot x dx}{\int \mu(x) dx} \tag{20}$$

Where Δq_o is the output laser power increment; x is the variable in the laser power increment membership function; $\mu(x)$ is the probability of the laser power increment. The simulation result is shown in figure 25.

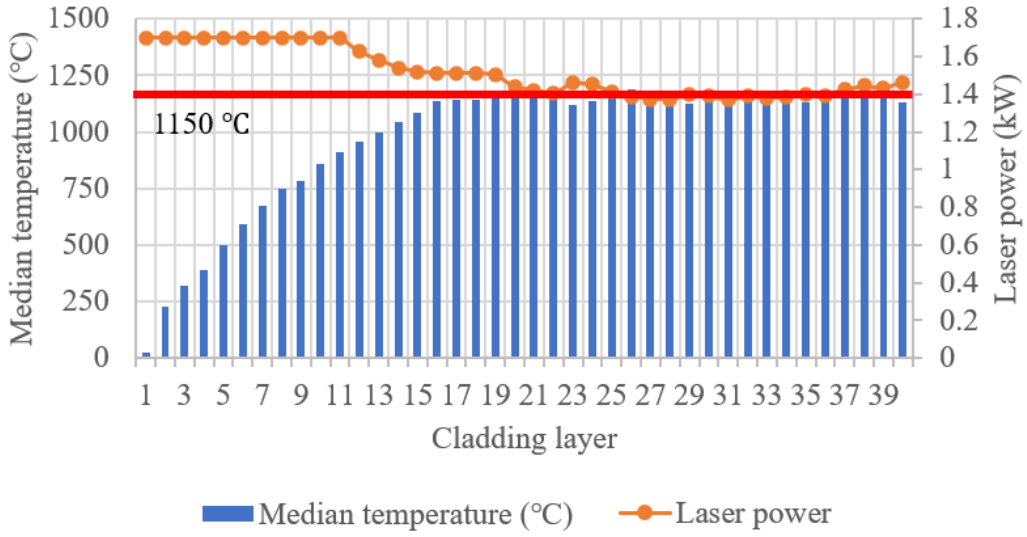

Figure 25. 25 mm square block with laser power control using fuzzy logic

A system is usually considered stabilized when the response of the system is within the error band, for which 2% is commonly used, and never leaves the error band again, thus the error band for the 25 mm square block is 22.5 ℃.

According to figure 25, after the median temperature exceeds 1150 ℃, the average deviation from the control objective is 24.3 ℃ and the standard deviation of the laser power is 0.035 kW. The cladding process is not fully stabilized by the standard of 2% error bandwidth but both deviations are in the category of 'small' by linguistic rule. Additionally, the controller has very limited responses because of the nature of the layer-wise control method. The fuzzy controller can be improved with better domain partition and more appropriate membership functions.

Unlike laser power control with fuzzy logic, the feed rate control with fuzzy logic is not particularly effective on the 25 mm square block. Although the energy flux into the clad is reduced by increasing the feed rate, the heat cycle is also reduced by increasing feed rate. For a small square block, the heat dissipation of the clad top surface is highly sensitive to the cooling time. Since the cooling time of the clad is inversely proportional to feed rate, the clad top surface median temperature is not necessarily decreasing with energy flux. The median temperature of 25 mm square block with various feed rates is presented in figure 26.

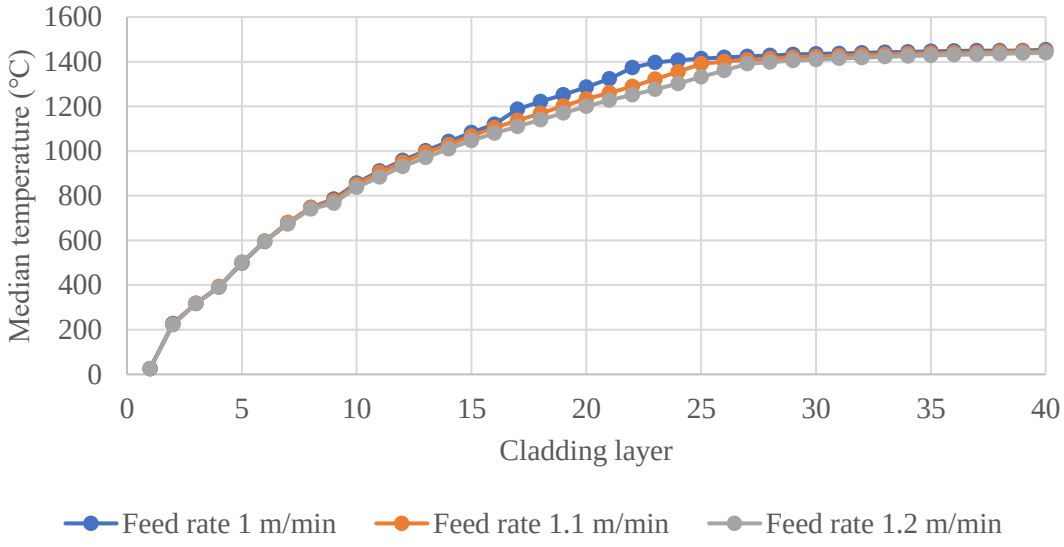

Figure 26. The median temperature of 25 mm square block workpiece with a various feed rate

According to figure 26, the median temperature of 1.0 m/min feed rate has very little difference with 1.2 m/min feed rate after 25 layers. Compared with the heat dissipation of clad top surface of 25 mm square block, the heat dissipation of clad top surface of the large square block is not sensitive to cooling time. For the 80 mm square block clad top surface, most of the energy is dissipated in the first 5 s, thus the median surface temperature is not strongly affected by cutting off 3 s cooling time. Therefore, the feed rate-based control can be used on a large workpiece to

improve the cladding efficiency and geometry accuracy, and laser power-based control should be used when the workpiece is too small for feed rate-based control to be effective.

Feed rate control can still improve the cladding efficiency when applied to the relatively large square model, whose dimension is listed in table 13. The control objective is to maintain the stabilized temperature at 700 ℃.

Table 13. 100 mm square block model dimension

	Length (mm)	Width (mm)	Height (mm)
Substrate	110	110	25
Clad	100	100	35

The membership function of the error and de/dl of feed rate control by fuzzy logic are the same as the laser power control. Similarly, the feed rate increment membership function also uses 'very large' to describe the 0.1 m/min increment, shown in figure 27. The clad is built in the center of the substrate as usual. The simulation result of the 100 mm square block model is presented in figure 28.

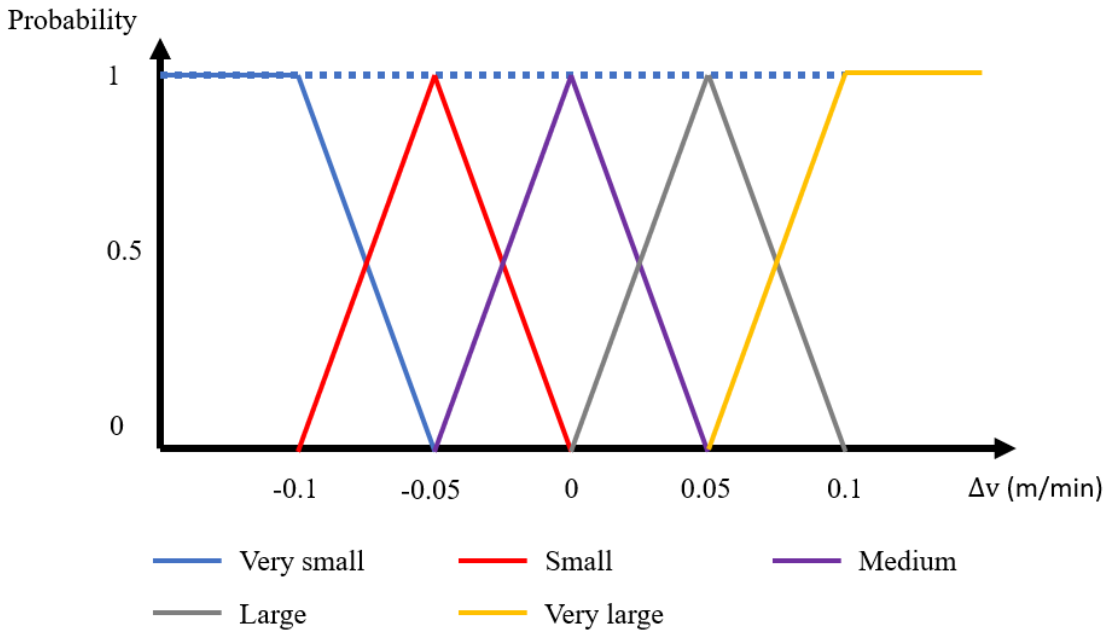

Figure 27. Membership function of feed rate increment

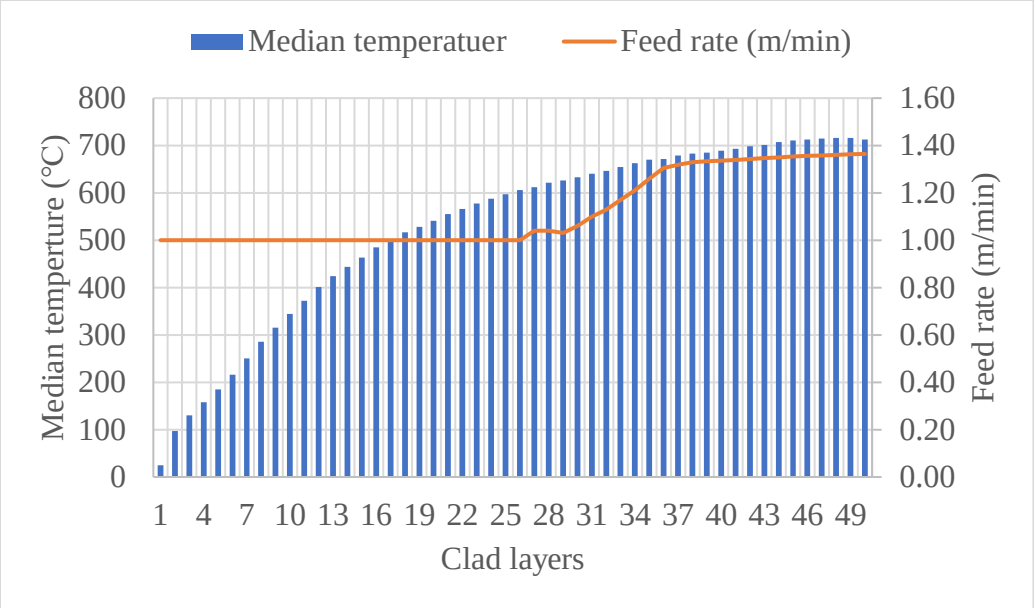

Figure 28. The feed rate-based control of the 100 mm square model

2.5 Discussion

For a 25 mm thin wall simulation, the melt pool energy can be controlled by either manipulating feed rate or laser power. The laser power-based control method can achieve better melt pool energy consistency, but the feed rate-based control is more time-efficient and the produced geometry size is closer to the expectation. Because there is a 2 s laser-off time between two consecutive layers in thin wall building process, the feed rate control is still effective for the 25 mm thin wall. Without the 2 s laser-off time, the feed rate control can no longer maintain the melt pool energy distribution nor median temperature.

As for the closed curve shape geometry simulation, such as square block, the fuzzy logic is used to control the laser power or feed rate of the next layer based on the information of existing layers. Because choosing the control method depends on the clad size and cladding parameters, it is beneficial to define a threshold temperature for choosing the control method.

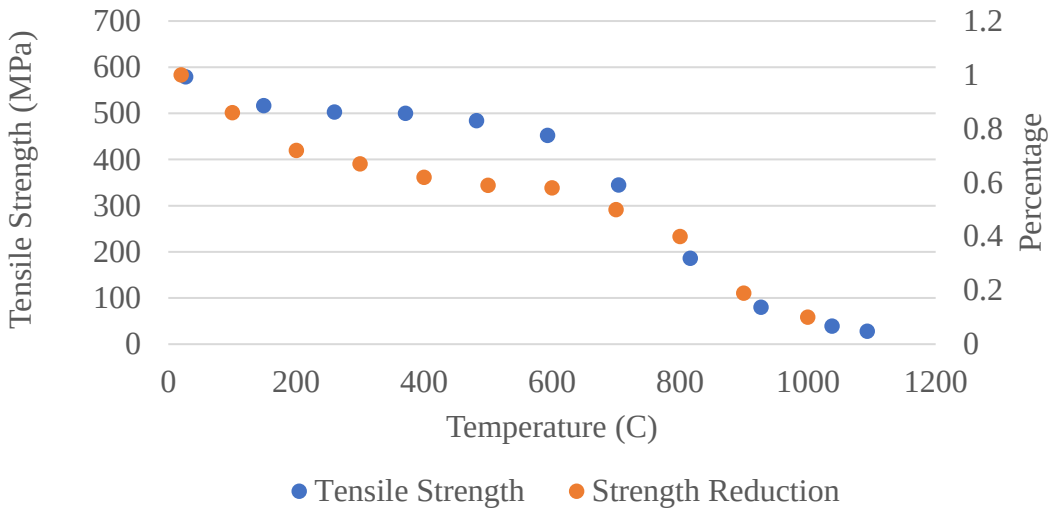

Figure 29. Temperature characteristic of the stainless steel 316L

According to figure 29, because the strength of stainless steel 316L is significantly reduced when the temperature is greater than 800 ℃, the median temperature of the clad top surface should be less than 800 ℃ to prevent potential deformation.

Furthermore, since the cladding process eventually can be stabilized without any control method knowing the relationship of the cladding parameter, clad size, and stabilized median temperature is helpful to maximize the cladding efficiency within the machine capacity. Equation 21, generated from curve fitting the date from a series of simulations of various workpiece sizes, laser power, and feed rate, can be used to determine the appropriate cladding parameters for a given closed-curve shape clad size.

$$f_T = f(d_p, q, v, \dot{m}) \tag{21}$$

Where d_p is the perimeter of the closed curved geometry; q is the laser power; v is the feed rate and $\dot{m}$ is the powder flow rate. The relationship is shown in figure 30 for the constant energy flux when feed rate and laser power are 1 m/min and 1.7 kW respectively.

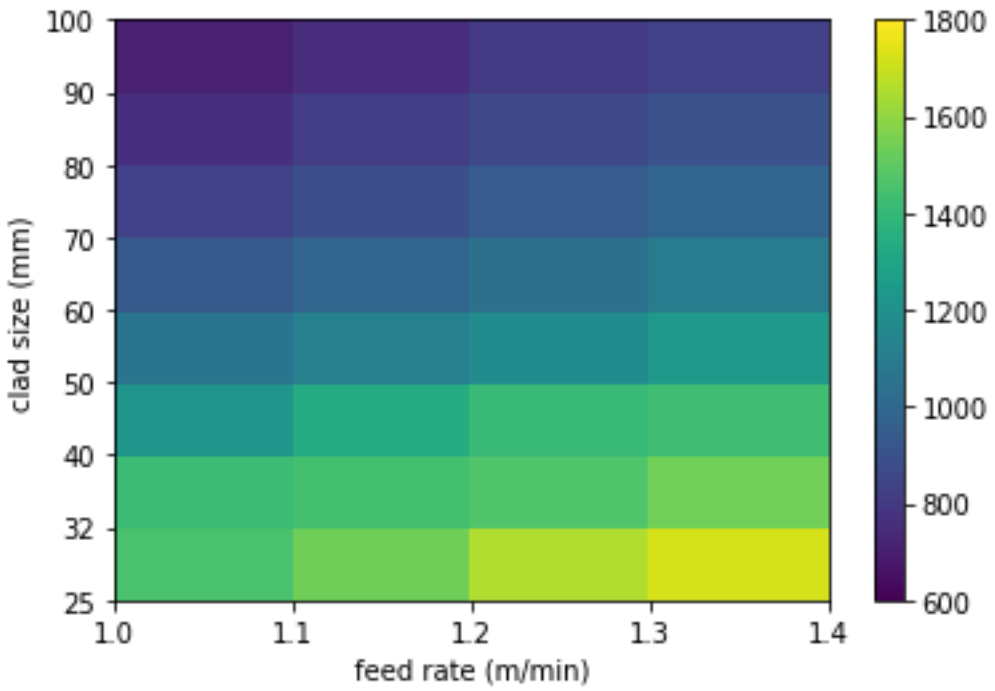

Figure 30. The relationship curve among stabilized median temperature, clad size, and cladding parameters

According to figure 30, since the stabilized temperature of 100 mm square block with static cladding parameters in table 14 is still less than 800 ℃, maximum cladding parameters can be used when building a closed curve part larger than 100 mm square. It should be noted that the maximum cladding parameters are based on 0.7 mm clad layer height.

Table 14. The maximum cladding parameters with 0.7 mm layer height

The maximum cladding parameters	
Laser power	2.5 kW
Feed rate	1.47m/min
Powder flow rate	34.5g/min

3. Simulation Techniques

A few simulation techniques are implanted to improve the simulation efficiency and accuracy.

3.1 Model Change Technique

Model change technique is often used when only a portion of the model is involved in a part of the simulation to save time or produce the desired shape by only showing different portions of the model at certain steps. In cladding simulation, the new layers are not included in the clad until the current layer is finished. Thus, the model change technique can be applied to activate layers when they are needed, figure 31. For a 32 layers thin wall, 34 steps are created to add a new layer to the clad at each step. (The extra 2 steps are the default initial step and user-defined initializing temperature step.)

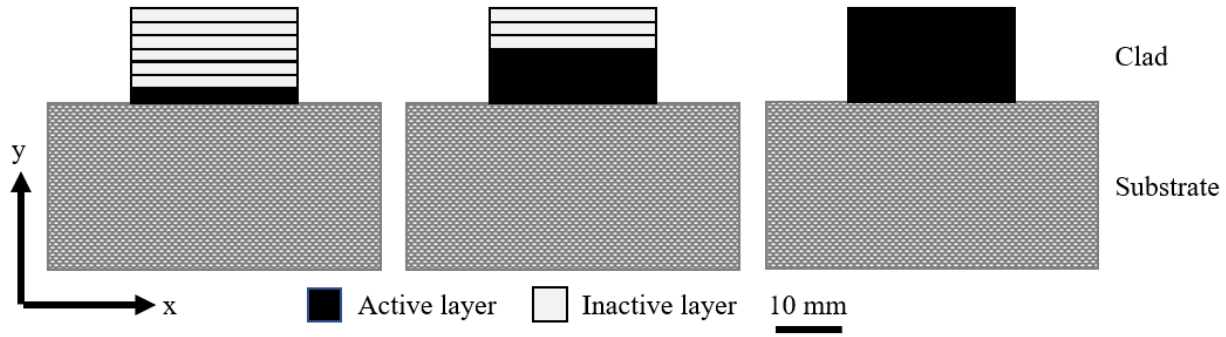

Figure 31. The initial (left), in progress (middle), finished status (right) of thin wall model with exaggerated clad height

The computational time saved by the model change technique mainly depends on the ratio of inactive elements number to total elements numbers. The simulation time is reduced by 17% for a thin wall model mentioned in section 2.3, while the simulation time is only reduced by 9% for a square block mentioned in section 2.4.

The cladding time needs to be predetermined to use the model change technique since model change needs to be defined in steps that require specific step time. Therefore, model change can be easily implanted in laser power-based control simulation because of the constant feed rate and cladding time on each layer, while new layers cannot be activated at each step in the feed rate-based control simulation because the cladding time cannot be predetermined.

3.2 Quiet Element Technique

Quiet element, also known as inactive element, is the element with nearly zero conductivity and performs as the air in the simulation. Once activated, the quiet element or inactive element has normal conductivity according to temperature. With the quiet element technique, the cladding process can be simulated as elements added to clad along with the laser spot movement. Compared with obtaining desired geometry by model change, the quiet element technique is closer to the actual cladding process because the elements are activated based on temperature instead of predetermined. On the other hand, the simulation efficiency cannot be improved by the quiet element technique since the inactive elements are still involved in the calculation.

As most of the details are explained in section 2.3, the inactive element is activated once 6 of the attached nodes to the element are active instead of all the attached nodes being active. This setup is a comprise of the inactive clad surface nodes due to large time increments and mesh size. Because some surface nodes may be included in the laser spot for only 1 increment with the time increment and mesh size setting mentioned in section 2.3, the clad surface nodes do not receive sufficient laser power to be activated. On the other hand, with a small mesh size and increment time, the surface nodes can receive adequate laser power, but the computational can be costly. In addition, except for clad surface nodes, the median temperature is barely impacted by the time

increment and mesh size. Therefore, to prevent excessive computational cost, the quiet or inactive element is activated based on 6 active attached nodes.

3.3 Convergence Settings

The default convergence settings of ABAQUS are designed to provide the reasonably optimal solution to nonlinear problems. The calculation result is accepted as converged if close enough to the exact solution. The approximation is rather strict in engineering standard when the default settings are used [31].

Since the convergence settings may create a certain variance from the exact solution, if less strict convergence criteria are applied, results can be not sufficiently close to the exact solution especially when the variance may accumulate along with the increments.

As mentioned in the previous section, the quiet element technique is implanted in simulation to improve accuracy, but also introduce the convergence issue because of the dual conductivity on the boundary nodes between an active element and inactive element, figure 32. The active node on the boundary has nearly zero conductivity in the inactive element to prevent conduction and has normal conductivity in an active element. With the default convergence setting, the result may not converge due to the excessive residual heat flux. The residual heat flux is usually caused by the temperature variance on the active boundary nodes. Because the temperature of the active boundary nodes around melt pool is generally between liquidus temperature and solidus temperature, even a small temperature variance may result in unresolved residual heat flux due to the latent heat.

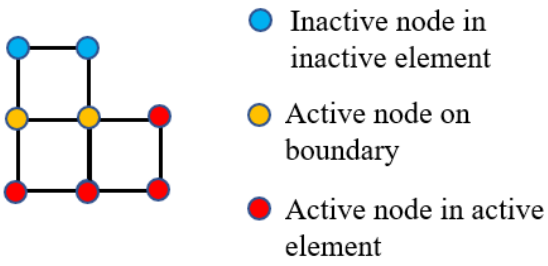

Figure 32. The boundary nodes with dual conductivity

Generally, the result of heat transfer simulation is considered converged if two criteria are met, which are the criterion for residual heat flux and the criterion for temperature correction. The criterion for residual heat flux is defined in equation 22 [31].

$$r_{max}^{a} \leq R_n^a \tilde{q}^a \tag{22}$$

Where a is the active field of heat transfer; r_{max}^{a} is the largest residual in balance equation for field a; R_n^a is the criterion for residual heat flux, 0.005 by default; $\tilde{q}^a$ is the overall time-averaged value of the heat flux for field a. The criterion for temperature correction is defined in equation 23. [1]

$$c_{max}^{a} \leq C_n^a \Delta u_{max}^{a} \tag{23}$$

Where c_{max}^{a} is the largest correction to any nodal variable; C_n^a is the criterion for temperature correction, 0.02 by default; Δu_{max}^{a} is the largest nodal temperature change.

The heat transfer simulation is sufficiently accurate when the default criterion of residual heat flux is met. But the simulation occasionally fails to converge because the residual heat flux cannot be reduced less than the criterion within the predetermined iterations. If the convergence criteria are not met, the increment time will be reduced and reattempted with D_H, 0.25 by default, times the current time increment. The process is repeated until the solution is found, or the simulation is

terminated because the time increment is reduced too many times. If a solution is found after time increment is reduced, the time increment is increased by a factor of D_D, 1.5 by default.

Because the largest temperature correction is neglectable compared with the nodal temperature when the criterion for residual heat flux is not met, the criterion for residual heat flux is increased from 0.005 to 0.01 to solve the convergence issue. The iteration controlling parameters, D_H and D_D, are assigned with new values to improve the simulation efficiency, which is summarized in table 15 along with the criterion for residual heat flux.

Table 15. The changed parameters to accelerate simulation

parameter	Default	New value	Benefits
R_n^α	0.005	0.01	The solution converges faster.
D_H	0.25	0.75	Time increment is reduced at a slower rate.
D_D	1.5	2	Time increment is back to initial value faster.

With settings in table 15, the simulation can complete without convergence issues and slightly fewer increments.

3.4 Fast Convergence Algorithm

In ABAQUS, the solution is found by the iterative method. For heat transfer simulation, the default initial guess of the solution is the temperature of the last increment, which works well when the material does not experience phase change in two consecutive increments. On the contrary, if the material is heated up from room temperature to solidus temperature, the default initial guess may cause the convergence issue because the initial guess is too far from the actual solution. To solve this issue, a fast convergence method is developed to find a solution closer to the actual solution in the early iterations. The solution is calculated by iterating equation 9 in section 2.1.

$$\left[\frac{1}{\Delta t}\int \rho \frac{dU}{dT}|_{t+\Delta t} dV + \int \frac{\partial N}{\partial x} k|_{t+\Delta t} dS + \int \frac{\partial h}{\partial T}(T - T_0) + h + 4\epsilon\sigma T^3 dS\right]\delta T \qquad (9)$$

$$= \int \dot{q}_v dV + \int \dot{q}_s dS - \frac{1}{\Delta t} \int \rho (U_{t+\Delta t} - U_t) dV - \int k|_t \frac{\partial T}{\partial x} dS$$

The material property including ρ, $\frac{dU}{dT}$, k, h and A are defined in UMATHT. If the left side of the equation is defined as M, equation 9 can be simplified as equation 24 by neglecting non-existent volume heat flux.

$$M \cdot V_n \cdot \delta T = \dot{q}_{in} - \frac{\Delta U \rho V_n}{\Delta t} - k_t \cdot \frac{\partial T}{\partial x} \cdot V_n \tag{24}$$

Where $\dot{q}_{in}$ is the incoming laser energy; V_n is the nodal volume. By properly defining internal energy difference in the second iteration, the iterative solver may produce a result closer to an actual solution than using the default initial guess, which reduces the number of iterations and solves the convergence issue without changing the convergence settings.

Since the fast convergence method is applied to all the nodes in the active field, most of the nodes need to go through the fast convergence method even though not experience the phase change in most of the increments, which causes unnecessary computational time. Therefore, the fast convergence method is not used in the simulation because of the excessive computational cost compared with changing convergence settings.

3.5 Disscussion

The simulation techniques are discussed in this chapter. Many articles use model change technique to active element based on the laser track location. In the actual cladding process, because the material is added to the clad on condition of melted instead of just being inside the laser track, the element activation based on temperature is closer to acutal cladding process than based on location in my perspective. The outcome difference might be negaletable for a small model, but the

outcome difference might be noteworthy by accumulation and needs to be further investigated for a large model.

Additionally, the simulation result is barely affected by changing the convergence criterion, because the nodal variance is small enough to ensure the accuracy. The mesh size and increment time has much greater impact on the simulation result than changing convergence criterion. Therefore, once the mesh size and increment time is determined, the baseline of simulation accuracy is settled.

4. Simulation in Python

To have a better knowledge of the stabilized status of the square block cladding process, a series of simulations need to be conducted with cladding parameters in table 16. The increment of each cladding parameter is 0.1 disregarding the unit. As mentioned in section 2.3, the powder flow rate is linearly proportional to the feed rate to keep the layer height constantly at 0.7 mm.

Table 16. The cladding parameters range of the simulation series

	Feed rate (m/min)	Laser power (kW)	Powder flow rate (g/min)
Range	1-1.4	1-1.7	23.5-32.9

In the simulations, the substrate height and clad height are constant at 25 mm and 35 mm respectively to eliminate the influence of the dimension difference other than length and width, which are the same in the simulation series. The length and width dimensions of the models are in listed in table 17.

Table 17. The model dimensions of simulation series

Clad (mm)	substrate (mm)
25	50
30	50
40	50
50	60
60	70
70	80
80	90
90	100
100	110

Running the simulations in ABAQUS is extremely costly both in time and storage space. A simulation with 110 mm substrate and 100 mm clad takes 314 hours and 144 gigabytes in ABAQUS. Thus, the python program is developed to run the simulations efficiently.

4.1 Heat Transfer Math Model

The heat transfer model in python program is based on nodes. The energy balance of a node is shown in equation 24.

$$\Delta T_n \rho V_n c_n = t_{incr}(p_L + \sum_{i=1}^{6} k_i A_i \frac{\partial T}{\partial X}|_i + \sum_{i=1}^{6} h_i A_i (T_n - T_0)) \quad (24)$$

Where ΔT_n is the nodal temperature increment of node n; T_i is the nodal temperature; ρ is the material density; V_n is the nodal volume; c_n is the specific heat at of node n; t_{incr} is the time increment; p_L is the incoming laser power; k_i is the conduction coefficient; A_i is the contact area of node n in direction i; h_i is the film coefficient in direction i; T_0 is the environmental temperature.

Similar to the ABAQUS simulation, the 'active' is also one of the material properties assigned to nodes. Since the energy balance equation is solved by direct solution instead of iterative method, the increment time needs to be reduced to ensure accuracy and stability [31]. The numerical simulation stability should meet the requirement of Fourier stability, equation 25.

$$\frac{k\Delta t}{(\Delta x)^2} \leq 0.5 \quad (25)$$

Where k is the conduction coefficient; Δt is the time increment; Δx is the mesh size. For the given mesh size Δx, the time increment should be small enough to ensure the stability for conduction. Meanwhile, to ensure the stability for the convection, the stability for convection should be satisfied, equation 26.

$$\frac{h\Delta t}{\Delta x} \leq 1.0 \quad (26)$$

Where h is the film coefficient. In consideration of the stability constraints, the mesh size is listed in table 18.

Table 18. The mesh size of python model

	Horizontal		Vertical		
Mesh size (mm)	Length	Width	Clad	Substrate top	Substrate bottom
	1	1	0.7	1	5

The substrate is meshed differently in a vertical direction because the substrate top, shown in figure 33, needs fine mesh to ensure the accuracy of the early layers of the clad. Meanwhile, the substrate bottom uses coarse mesh to avoid the unnecessary computational cost. Based on the mesh size in table 18, the time increment needs to be 0.01 s to maintain simulation stabilized. With the mesh setting in table 18 and 0.01 increment time, the python program produces a very similar result with ABAQUS simulation after a few layers. (2-5 layers depending on the model size.)

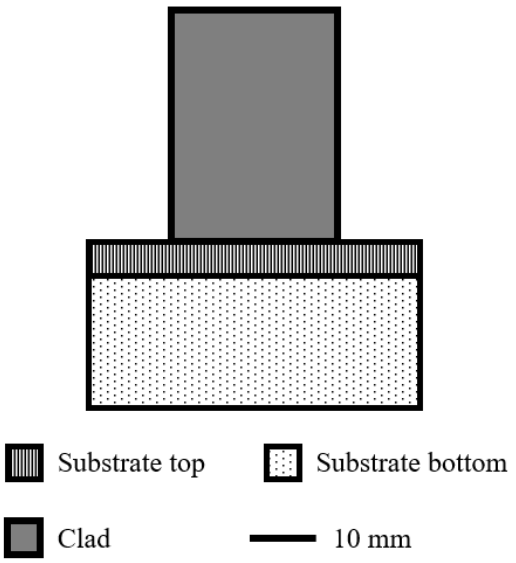

Figure 33. The mesh difference between substrate top and bottom

For the same simulation with 110 mm substrate and 100 mm clad, it takes 77 hours for the python program to complete, which reduces the running time by 75.5% compared with ABAQUS. The time reduced by python largely depends on the size of the model. Generally, the saved time percentage is increasing with the model size.

4.2 Unsolved Issues in Simulation

Although the python program is relative more efficient compared with ABAQUS simulation, the simulation of the 100 mm square model still takes more than 1 day to finish. One way to increase the efficiency is to use the multi-processing feature in python. By using multi-processing, theoretically, the simulation can be reduced proportionally to the number of processers being used. But the multi-processing has an over-head time which prolongs the simulation depending on the number of increments.

5. Experiment

To test the effectiveness of the energy control method~~, a contrast experiment~~ deposition experiments were pefromed. ~~of the thin wall with feed rate control and with laser power control is conducted including thin wall without any control method, with feed rate-based control, and with laser power-based control.~~ Thin walls were printed without control, with laser power control, with feed rate control, and with a combined laser power and feed rate control.

To further test the control method on more workpiece shapes and validate the temperature threshold of the closed curve shape, a series of square block experiments are conducted.

5.1 Experiment Set-Up

The experiment is conducted on Lasertec 65 Hybrid as mentioned previously. Because powder flow rate needs to be changed during the experiment, the dynamics powder splitter system is used to adjust the powder flow rate dynamically between two layers.

5.1.1 Machine Set-Up

The powder splitter is installed on the laser head, figure 34, to control the powder flow before the powder enters the nozzle. The laser power is controlled directly by the G code.

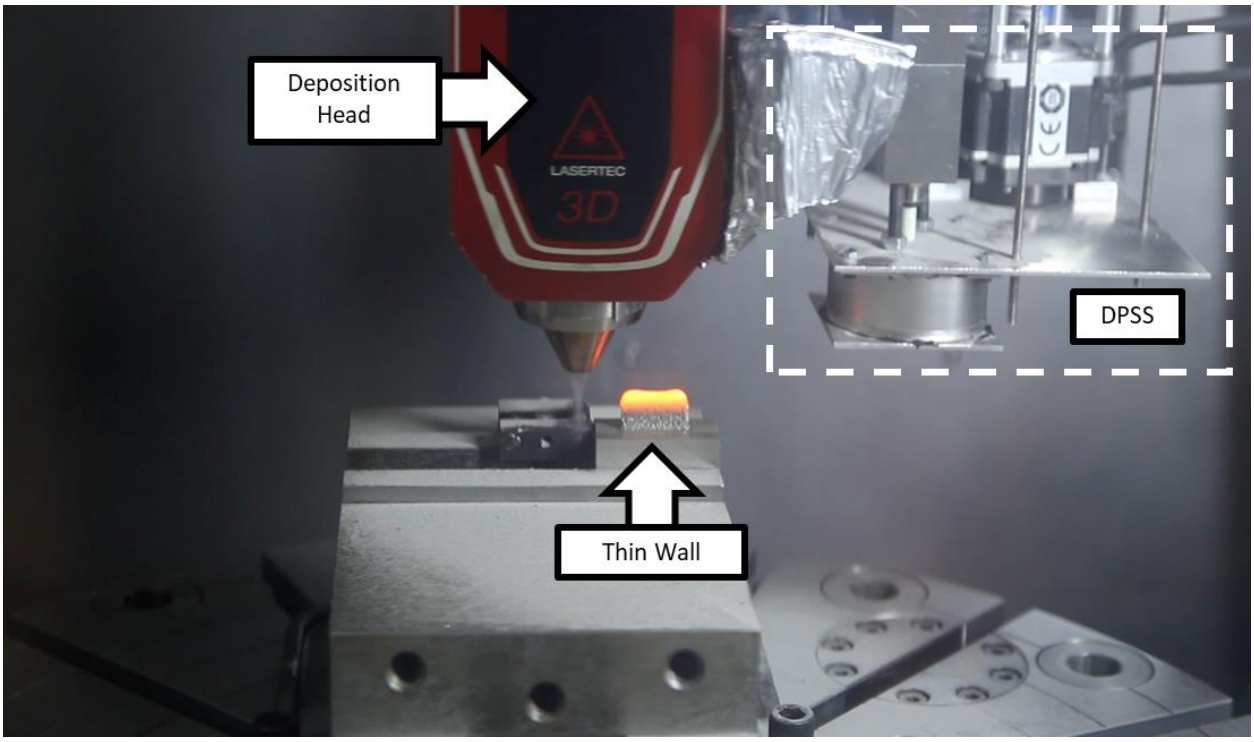

Figure 34. Experiment set up for thin wall cladding with powder splitter

5.1.2 Input Data

The data generated from simulation is used in the experiment for validation. For the laser power control simulation, the laser power data is directly coded in the G code. On the other hand, the data from thin wall feed rate control simulation is merged into 8 numbers first due to the limitation of powder splitter, then coded into G code. Meanwhile, the powder flow rate is also changed proportionally to the feed rate to keep the powder flux constant.

5.1.3 Thin wall melt pool energy control experiment

The experiment data is presented in table 19 and figure 35.

Table 19. Experiment data generated from simulation

Layer	Laser Power Control		Feed Rate Control			
	Laser Power (kW)	EF $\left(\frac{J}{mm^2}\right)$	Feed rate $\left(\frac{m}{min}\right)$	Powder Flow Rate $\left(\frac{g}{min}\right)$	EF $\left(\frac{J}{mm^2}\right)$	PF $\left(\frac{\mu g}{mm^2}\right)$
1	1.70	34.0	1.00	23.50	34.0	7.8
2	1.70	34.0	1.00	23.50	34.0	7.8
3	1.70	34.0	1.00	23.50	34.0	7.8
4	1.70	34.0	1.00	23.50	34.0	7.8
5	1.62	32.3	1.19	28.00	28.5	7.8
6	1.52	30.3	1.19	28.00	28.5	7.8
7	1.44	28.8	1.19	28.00	28.5	7.8
8	1.37	27.4	1.44	34.00	23.5	7.8
9	1.32	26.3	1.44	34.00	23.5	7.8
10	1.25	25.0	1.44	34.00	23.5	7.8
11	1.22	24.4	1.59	37.50	21.3	7.8
12	1.18	23.5	1.59	37.50	21.3	7.8
13	1.14	22.7	1.74	41.00	19.5	7.8
14	1.12	22.3	1.74	41.00	19.5	7.8
15	1.09	21.8	1.74	41.00	19.5	7.8
16	1.07	21.3	1.89	44.50	18.0	7.8
17	1.03	20.6	1.89	44.50	18.0	7.8
18	1.01	20.1	1.89	44.50	18.0	7.8
19	1.00	20.0	2.00	47.00	17.0	7.8
20	0.99	19.7	2.00	47.00	17.0	7.8
21	0.97	19.4	2.00	47.00	17.0	7.8
22	0.94	18.8	2.00	47.00	17.0	7.8
23	0.93	18.5	2.14	50.50	15.8	7.8
24	0.93	18.6	2.14	50.50	15.8	7.8
25	0.92	18.4	2.14	50.50	15.8	7.8
26	0.91	18.1	2.14	50.50	15.8	7.8
27	0.90	17.9	2.14	50.50	15.8	7.8
28	0.87	17.4	2.14	50.50	15.8	7.8
29	0.88	17.6	2.14	50.50	15.8	7.8
30	0.88	17.5	2.14	50.50	15.8	7.8
31	0.87	17.3	2.14	50.50	15.8	7.8
32	0.87	17.4	2.14	50.50	15.8	7.8

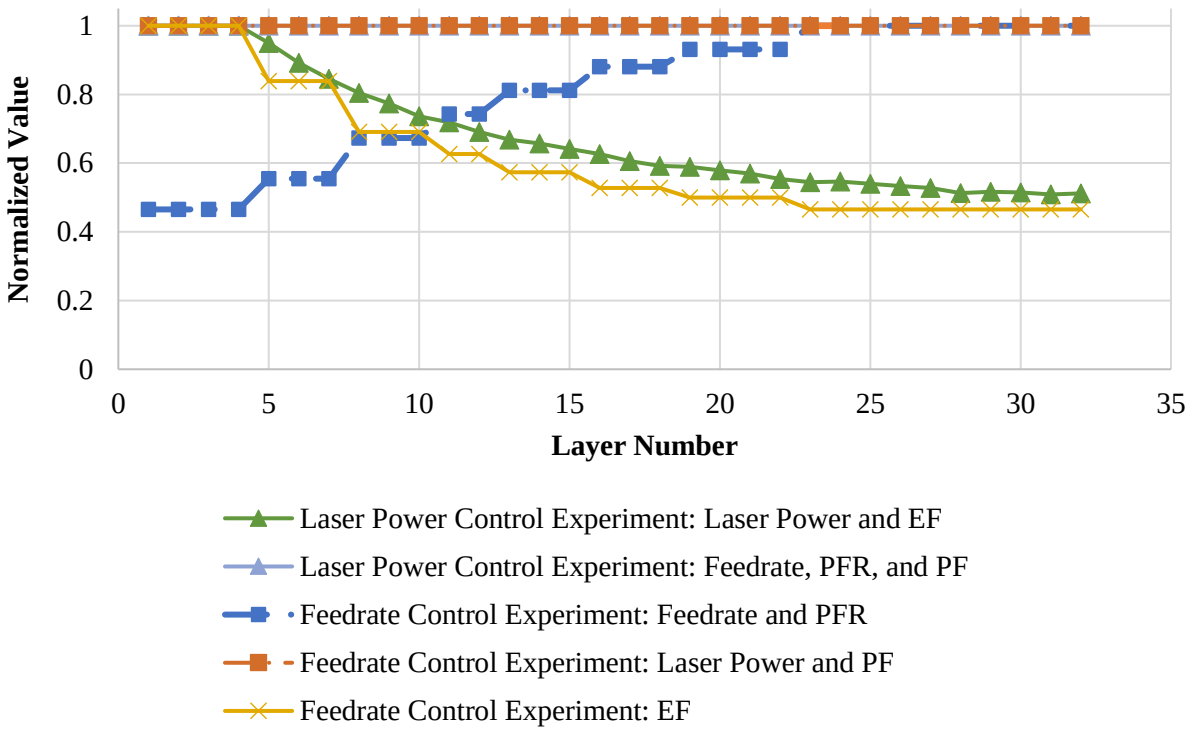

Figure 35. Cladding parameters for thin wall melt pool energy control experiments of laser power control and feed rate control

Both thin wall with melt pool energy control experiment results shows better geometry consistency compared with thin wall experiment with static cladding parameters. The thin wall width variance is significantly reduced by the melt pool energy control method. The thin wall height without control is shorter than the expected height, 22.4 mm, due to the over-heated upper side layers, which is also amended by melt pool energy control. The comparison of the thin walls is presented in figure 36.

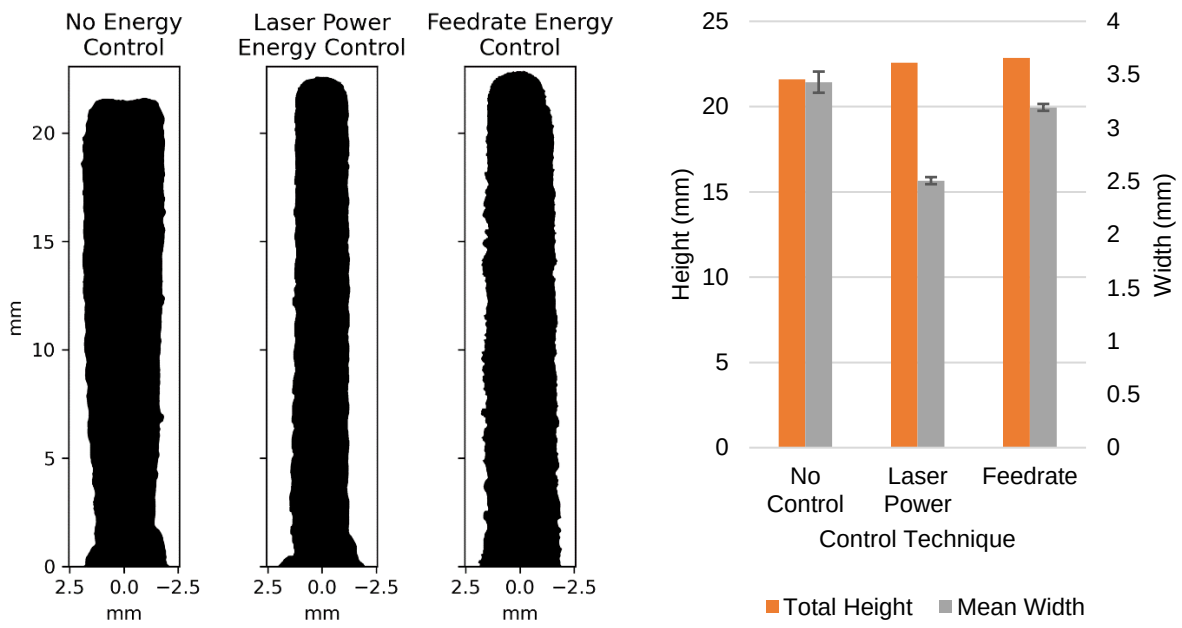

a) b)

Figure 36. Comparison of thin wall clad with no control, melt pool energy control by laser power method and melt pool energy control by feed rate method a) image taken by MicroVu Excel HC502 and b) comparison between heigh, width, and width variation

The outlines of original thin wall images are obscure and, therefore need to be processed, figure 37.

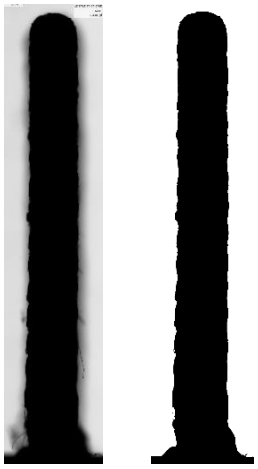

a) b)

Figure 37. The melt pool energy control by laser power method thin wall image a) before and b) after processed

Each pixel color can be represented by 3 numbers range from 0 to 255, also known as RBG values. The pixel color can be converted to grey degree by equation 27.

$$v_{grey} = p_0 * 0.299 + p_1 * 0.587 + p_2 * 0.114 \quad (27)$$

Where v_{grey} is the grey value; p_0, p_1, p_2 are the RBG values. The pixel color after converting is (v_{grey}, v_{grey}, v_{grey}). Because the grey degree of most of the thin wall center pixels is less than 24, 24 is set to be the threshold to filter the background pixel from thin wall pixel.

Although the geometry consistency can be improved by both melt pool energy control methods, the experiment result shows the difference between the laser power-based control method and feed rate-based control method regrading to the clad width. The average clad width of the feed rate-based control method, 2.9 mm, is closer to the expected clad width, 3 mm, than the laser power-based control method, 2.5 mm. Even though the melt pool energy distribution of both methods is similar, the layers with feed rate-based control method cool down slower than with laser power-

based control method, which keeps the layers at high temperature for a longer time and allows more powder to melt. Therefore, other than time efficiency, feed rate-based control method also has better powder efficiency and geometry consistency than laser power-based method.

5.1.4 Square block

The setup and data pre-processing of square block experiment are the same as the thin wall experiment. The 100 mm square block experiment is conducted to test the effectiveness of feed rate control. The cladding parameters are listed in table 20. Because the power splitter can only take in 16 values, therefore, the feed rate and powder flow rate values are merged into 16 values respectively.

Table 20. The cladding parameters of the feed rate control of 100 mm square block

Layer	Laser power	Original Feed Rate	Feed Rate Reduced to 16 values	Original Powder Flow Rate	Powder Flow Rate Reduced to 16 values
Unit	kW	m/min	m/min	g/min	g/min
1	1.7	1	1	23.5	23.5
2	1.7	1	1	23.5	23.5
3	1.7	1	1	23.5	23.5
4	1.7	1	1	23.5	23.5
5	1.7	1	1	23.5	23.5
6	1.7	1	1	23.5	23.5
7	1.7	1	1	23.5	23.5
8	1.7	1	1	23.5	23.5
9	1.7	1	1	23.5	23.5
10	1.7	1	1	23.5	23.5
11	1.7	1	1	23.5	23.5
12	1.7	1	1	23.5	23.5
13	1.7	1	1	23.5	23.5
14	1.7	1	1	23.5	23.5
15	1.7	1	1	23.5	23.5
16	1.7	1	1	23.5	23.5
17	1.7	1	1	23.5	23.5
18	1.7	1	1	23.5	23.5

19	1.7	1	1	23.5	23.5
20	1.7	1	1	23.5	23.5
21	1.7	1	1	23.5	23.5
22	1.7	1	1	23.5	23.5
23	1.7	1	1	23.5	23.5
24	1.7	1	1	23.5	23.5
25	1.7	1	1	23.5	23.5
26	1.7	1	1	23.5	23.5
27	1.7	1.0398	1.04	24.4353	24.67
28	1.7	1.0398	1.04	24.4353	24.67
29	1.7	1.0302	1.03	24.2097	24.09
30	1.7	1.0602	1.06	24.9147	24.67
31	1.7	1.0998	1.1	25.8453	25.82
32	1.7	1.1298	1.13	26.5503	26.39
33	1.7	1.17	1.17	27.495	27.52
34	1.7	1.2102	1.21	28.4397	28.62
35	1.7	1.25946	1.26	29.59731	29.69
36	1.7	1.30548	1.31	30.67878	30.73
37	1.7	1.31862	1.32	30.98757	30.73
38	1.7	1.32912	1.33	31.23432	31.23
39	1.7	1.33314	1.33	31.32879	31.23
40	1.7	1.33644	1.34	31.40634	31.23
41	1.7	1.33896	1.34	31.46556	31.23
42	1.7	1.34244	1.34	31.54734	31.73
43	1.7	1.34622	1.35	31.63617	31.73
44	1.7	1.35012	1.35	31.72782	31.73
45	1.7	1.3542	1.35	31.8237	31.73
46	1.7	1.35666	1.36	31.88151	31.73
47	1.7	1.3581	1.36	31.91535	31.73
48	1.7	1.36032	1.36	31.96752	31.73
49	1.7	1.36266	1.36	32.02251	32.21
50	1.7	1.36422	1.36	32.05917	32.21

A series of square block experiments with static cladding parameters are conducted to test the influence of temperature threshold for square block geometry consistency. The static cladding parameters and square model dimensions are listed in table 21 and table 22.

Table 21. Static cladding parameters of square block

Laser Power (kW)	Feed Rate (m/min)	Powder Flow Rate (g/min)
1.7	1	23.5

Table 22. The dimension of the square block series

Substrate Height (mm)	Substrate Length (mm)	Substrate Length in Simulation (mm)	Clad Height (mm)	Clad Length (mm)
25	110	50	35	25
25	110	50	35	32
25	110	50	35	40
25	110	60	35	50
25	110	70	35	60
25	110	80	35	70
25	110	90	35	80
25	110	100	35	90
25	110	110	35	100

A few square block experiments share the same substrate to save substrate. The small square block is deposited on the substrate first and the large square block is deposited after the small square block fully cooling down to room temperature. The substrate sizes of the experiment are mostly different from the simulation, but the influence of the substrate size difference is very limited, especially for the upper layers.

The 100 mm square block experiment results are shown in figure 38.

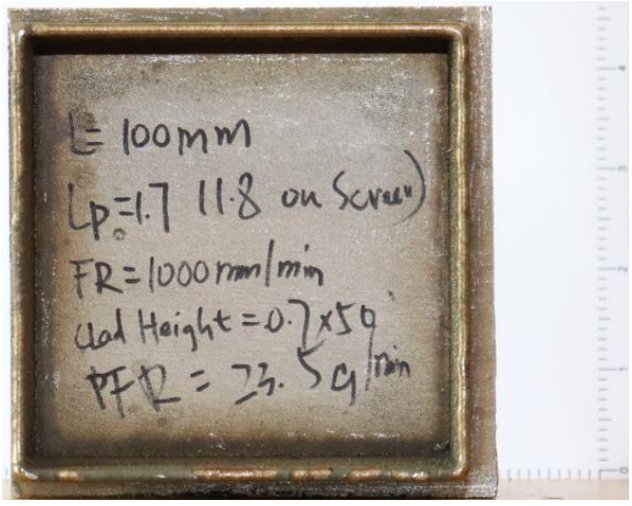

a) 100 mm square block with static cladding parameters

b) 100 mm square block with feed rate control (the clad outside); 32 mm square block (the clad inside)

c) 100 mm square block with maximum cladding parameters

Figure 38. The comparison among a) 100 mm square block with static cladding parameters, b) 100 mm square block with feed rate control and c) 100 mm square block with maximum cladding parameters

The square block experiment results with various clad sizes are showed in figure 39.

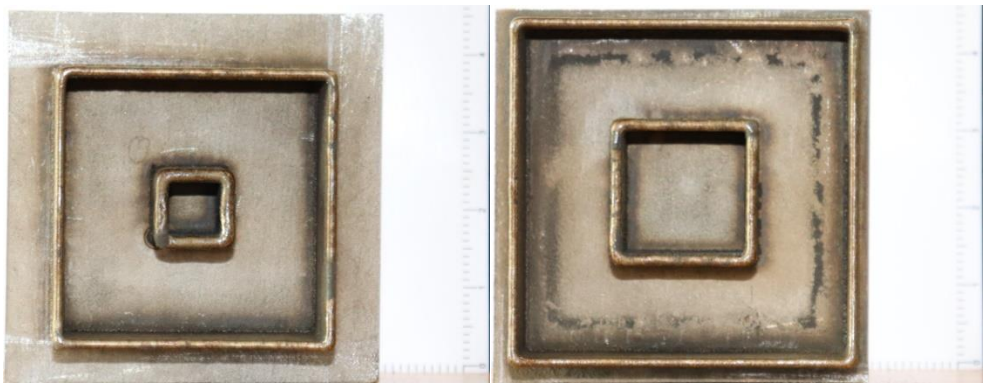

a) b)

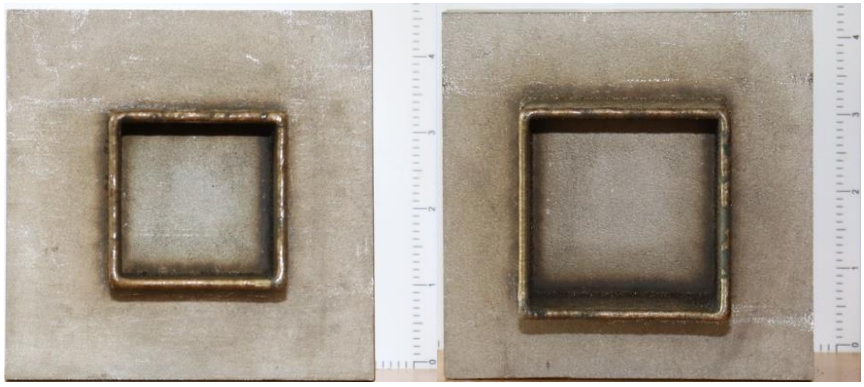

c) d)

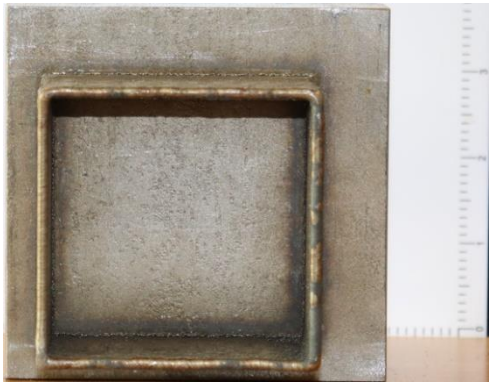

e)

Figure 39. The square blocks of a) 25 mm (inside) and 80 mm (outside), b) 40 mm (inside) square block, c) 50 mm, d) 60 mm and e) 70 mm

Because the square blocks are only processed with file and sandpaper, the surfaces are still uneven due to the metal particles and thus the measurements are larger than the actual sizes. The width and height of square blocks are measured in the middle of each side of the clad and their average value is listed in table 23.

Table 23. The clad width of square block experiments

Square block size (mm)	Deposition method	Clad width (mm)	Clad height (mm)
25	Static cladding parameters	4.1	36.8
32	Static cladding parameters	3.7	36.3
40	Static cladding parameters	3.6	35.7
50	Static cladding parameters	3.5	35.5
60	Static cladding parameters	3.5	35.8
70	Static cladding parameters	3.5	35.3
80	Static cladding parameters	3.4	35.5
100	Static cladding parameters	3.4	35.3
100	Max cladding parameters	3.3	32.7
100	Feed rate control	3.4	35.9

5.2 Discussion

~~From the experiment results with static cladding parameters, i~~It can be concluded from the experimental results that static cladding parameters will yield deformed parts if the clad size is small. In addition, it should be noted that even if the clad size is smaller than 70 mm~~,~~ whose median temperature of the top surface is greater than 800 ℃ in simulation~~,~~ the clad is not necessarily deformed. The clad height of the 100 mm square block with maximum cladding parameters is highly varied. The corner height is taller than the middle height by 2.7 mm on average. Meanwhile, the clad width is relatively consistent compared with clad height. No obvious inconsistency is observed in width.

6. Summary

This study is focused on improving DED productivity and geometric accuracy. Both laser power-based and feed rate-based energy control methods are developed by conducting thin wall simulation and validated by the experiment first. Both energy control methods can obtain geometric consistency, and feed rate-based control can also improve productivity. However, the square block simulation reveals that the feed rate-based control method is ineffective when the heat cycle is too short per layer due to limited clad size, which causes the surface temperature to be greater than the threshold temperature. The laser power-based control method is needed when the heat cycle is too short for the feed rate-based control method to maintain proper surface temperature. Therefore, to achieve the highest productivity while maintaining geometric accuracy, the deposition strategy should be determined according to the deposition status.

Additionally, the model change and quite element technique are used in the script to improve the simulation efficiency. Also, the convergence parameters are changed to accommodate the needs of special situations. A series of simulations are conducted to learn the relationship among the clad size, cladding parameters, and stabilized median surface temperature. The python program is developed to further improve the simulation efficiency considering the simulation. The findings of the simulations are listed below:

- The thin wall clad is deformed with static recommended cladding parameters if there is no sufficient interlayer dwell time.
- The thin wall clad can be improved by both feed rate control and laser power control method. Feed rate control can produce geometry size closer to expected value than laser power control and has better cladding efficiency.

- The simulation efficiency and accuracy is improved by simulation techniques and python program.
- The closed curve shape clad is deformed with static cladding parameters given no interlayer dwell time. The clad geometry can be improved by both laser power control and feed rate control method, but feed rate control method is not effective when the size is small.
- Choosing control method is based on the stabilized median temperature. The stabilized median temperature should be than the threshold, 800 ℃, to avoid the penitential deformation.
- The relationship among clad size, cladding parameters and stabilized median surface temperature is found by simulations.

7. Future Work

Because a great amount of this study is related to simulation, improving simulation efficiency can be very helpful. Running a simulation in python is much faster than in ABAQUS for simple geometries such as thin wall and square blocks. But the python program still has the potential to further improve the simulation speed. One of the options is using multiprocessing or multi-thread. However, the overhead time of multiprocessing can slow down the simulation drastically. In the future, hopefully this issue can be solved.

The equation 21 which describes the relationship of cladding parameter, clad dimension and stabilized temperature is not complete due to insufficient data. Only the relationship of constant energy flux is presented in figure 30. The complete relationship requires more simulation data and faster simulation speed.

In addition, the cladding process control can be extended to more complicated geometries. The cladding process of any arbitrary geometry can be improved by either laser power control or feed rate control according to the clad size. For instance, if the horizontal clad size is decreasing with clad height, the laser power control should be used to prevent from overheated. On the other hand, if the clad size is large, the feed rate control should be used to improve the efficiency. A new method in python will be developed to describe an arbitrary geometry. And similar to the current study, offline control will be studied in the simulation, which produces data for experiment validation.

Reference

[1] P. K. Gokuldoss, S. Kolla, and J. Eckert, "Additive manufacturing processes: Selective laser melting, electron beam melting and binder jetting-selection guidelines," *Materials (Basel).*, vol. 10, no. 6, 2017, doi: 10.3390/ma10060672.

[2] A. Saboori, A. Aversa, G. Marchese, S. Biamino, M. Lombardi, and P. Fino, "Application of directed energy deposition-based additive manufacturing in repair," *Appl. Sci.*, vol. 9, no. 16, 2019, doi: 10.3390/app9163316.

[3] W. T. Nugroho, Y. Dong, and A. Pramanik, *3D printing composite materials: A comprehensive review*. Elsevier Ltd., 2021.

[4] S. L. Sing, C. F. Tey, J. H. K. Tan, S. Huang, and W. Y. Yeong, *3D printing of metals in rapid prototyping of biomaterials: Techniques in additive manufacturing*, Second Edi. Elsevier Ltd., 2019.

[5] W. Liu and J. N. DuPont, "Fabrication of functionally graded TiC/Ti composites by laser engineered net shaping," *Scr. Mater.*, vol. 48, no. 9, pp. 1337–1342, 2003, doi: 10.1016/S1359-6462(03)00020-4.

[6] S. Wolff, T. Lee, E. Faierson, K. Ehmann, and J. Cao, "Anisotropic properties of directed energy deposition (DED)-processed Ti–6Al–4V," *J. Manuf. Process.*, vol. 24, pp. 397–405, 2016, doi: 10.1016/j.jmapro.2016.06.020.

[7] Y. Kakinuma *et al.*, "Influence of metal powder characteristics on product quality with directed energy deposition of Inconel 625," *CIRP Ann. - Manuf. Technol.*, vol. 65, no. 1, pp. 209–212, 2016, doi: 10.1016/j.cirp.2016.04.058.

[8] V. Fallah, M. Alimardani, S. F. Corbin, and A. Khajepour, "Temporal development of melt-pool morphology and clad geometry in laser powder deposition," *Comput. Mater. Sci.*, vol. 50, no. 7, pp. 2124–2134, 2011, doi: 10.1016/j.commatsci.2011.02.018.

[9] W. M. Steen and J. Mazumder, *Laser Material Processing*, 4th ed. London: Springer-Verlag London Ltd., 2010.

[10] J. Paulo Davim, C. Oliveira, and A. Cardoso, "Predicting the geometric form of clad in laser cladding by powder using multiple regression analysis (MRA)," *Mater. Des.*, vol. 29, no. 2, pp. 554–557, 2008, doi: 10.1016/j.matdes.2007.01.023.

[11] H. Tan, J. Chen, F. Zhang, X. Lin, and W. Huang, "Process analysis for laser solid forming of thin-wall structure," *Int. J. Mach. Tools Manuf.*, vol. 50, no. 1, pp. 1–8, 2010, doi: 10.1016/j.ijmachtools.2009.10.003.

[12] L. Leung, "Investigation of high-speed directed energy deposition (DED) for geometric accuracy and productivity," University of California, Davis, 2019.

[13] D. Mori, "Additive manufacturing-Reinvent your metal production." https://en.dmgmori.com/products/machines/additive-manufacturing/powder-nozzle/lasertec-65-ded-hybrid%0Ahttps://en.dmgmori.com/resource/blob/71066/db7d4d589d66c2838c9570d4eee

3ac03/pl0uk-additive-manufacturing-pdf-data.pdf.

[14] L.Markusson, “Powder characterization for additive manufacturing processes,” *Luleå Univ. Technol.*, no. January 2019, p. 128, 2017.

[15] J. I. Arrizubieta, A. Lamikiz, F. Klocke, S. Martínez, K. Arntz, and E. Ukar, “Evaluation of the relevance of melt pool dynamics in Laser Material Deposition process modeling,” *Int. J. Heat Mass Transf.*, vol. 115, pp. 80–91, 2017, doi: 10.1016/j.ijheatmasstransfer.2017.07.011.

[16] C. Lalas, K. Tsirbas, K. Salonitis, and G. Chryssolouris, “An analytical model of the laser clad geometry,” *Int. J. Adv. Manuf. Technol.*, vol. 32, no. 1–2, pp. 34–41, 2007, doi: 10.1007/s00170-005-0318-0.

[17] M. Picasso, C. F. Marsden, J. D. Wagniere, A. Frenk, and M. Rappaz, “A simple but realistic model for laser cladding,” *Metall. Mater. Trans. B*, vol. 25, no. 2, pp. 281–291, 1994, doi: 10.1007/BF02665211.

[18] A. J. Pinkerton and L. Li, “Modelling the geometry of a moving laser melt pool and deposition track via energy and mass balances,” *J. Phys. D. Appl. Phys.*, vol. 37, no. 14, pp. 1885–1895, 2004, doi: 10.1088/0022-3727/37/14/003.

[19] P. Peyre, P. Aubry, R. Fabbro, R. Neveu, and A. Longuet, “Analytical and numerical modelling of the direct metal deposition laser process,” *J. Phys. D. Appl. Phys.*, vol. 41, no. 2, 2008, doi: 10.1088/0022-3727/41/2/025403.

[20] E. Soylemez, J. L. Beuth, and K. Taminger, “Controlling melt pool dimensions over a wide range of material deposition rates in electron beam additive manufacturing,” *21st Annu. Int. Solid Free. Fabr. Symp. - An Addit. Manuf. Conf. SFF 2010*, no. June, pp. 571–582, 2010.

[21] H. Qi, M. Azer, and P. Singh, “Adaptive toolpath deposition method for laser net shape manufacturing and repair of turbine compressor airfoils,” *Int. J. Adv. Manuf. Technol.*, vol. 48, no. 1–4, pp. 121–131, 2010, doi: 10.1007/s00170-009-2265-7.

[22] W. Hofmeister and M. Griffith, “Solidification in direct metal deposition by LENS processing,” *Jom*, vol. 53, no. 9, pp. 30–34, 2001, doi: 10.1007/s11837-001-0066-z.

[23] L. Song and J. Mazumder, “Feedback control of melt pool temperature during laser cladding process,” *IEEE Trans. Control Syst. Technol.*, vol. 19, no. 6, pp. 1349–1356, 2011, doi: 10.1109/TCST.2010.2093901.

[24] Y. Sun and M. Hao, “Statistical analysis and optimization of process parameters in Ti6Al4V laser cladding using Nd:YAG laser,” *Opt. Lasers Eng.*, vol. 50, no. 7, pp. 985–995, 2012, doi: 10.1016/j.optlaseng.2012.01.018.

[25] F. Meriaudeau and F. Truchetet, “Control and optimization of the laser cladding process using matrix cameras and image processing,” *J. Laser Appl.*, vol. 8, no. 6, pp. 317–324, 1996, doi: 10.2351/1.4745438.

[26] G. Bi, B. Schürmann, A. Gasser, K. Wissenbach, and R. Poprawe, “Development and qualification of a novel laser-cladding head with integrated sensors,” *Int. J. Mach. Tools*

Manuf., vol. 47, no. 3–4, pp. 555–561, 2007, doi: 10.1016/j.ijmachtools.2006.05.010.

[27] P. A. Vetter, T. Engel, and J. Fontaine, "Laser cladding: the relevant parameters for process control," *Laser Mater. Process. Ind. Microelectron. Appl.*, vol. 2207, no. September 1994, p. 452, 1994, doi: 10.1117/12.184751.

[28] A. Calleja, I. Tabernero, A. Fernández, A. Celaya, A. Lamikiz, and L. N. López De Lacalle, "Improvement of strategies and parameters for multi-axis laser cladding operations," *Opt. Lasers Eng.*, vol. 56, pp. 113–120, 2014, doi: 10.1016/j.optlaseng.2013.12.017.

[29] W. Devesse, D. De Baere, and P. Guillaume, "Design of a model-based controller with temperature feedback for laser cladding," *Phys. Procedia*, vol. 56, no. C, pp. 211–219, 2014, doi: 10.1016/j.phpro.2014.08.165.

[30] P. Koruba, K. Wall, and J. Reiner, "Influence of processing gases in laser cladding based on simulation analysis and experimental tests," *Procedia CIRP*, vol. 74, pp. 719–723, 2018, doi: 10.1016/j.procir.2018.08.025.

[31] Simula, "Abaqus 6.12 User's Manual." 2012.

[32] W. Stopyra, J. Kurzac, K. Gruber, T. Kurzynowski, and E. Chlebus, "Influence of laser power on the penetration depth and geometry of scanning tracks in selective laser melting," *Laser Technol. 2016 Prog. Appl. Lasers*, vol. 10159, no. December 2016, p. 101590R, 2016, doi: 10.1117/12.2262079.

[33] A. Frenk, M. Vandyoussefi, J.-D. Wagnière, W. Kurz, and A. Zryd, "Analysis of the laser-cladding process for stellite on steel," *Metall. Mater. Trans. B*, vol. 28, no. 3, pp. 501–508, 1997, doi: 10.1007/s11663-997-0117-0.

[34] F. Wirth, D. Eisenbarth, and K. Wegener, "Absorptivity measurements and heat source modeling to simulate laser cladding," *Phys. Procedia*, vol. 83, pp. 1424–1434, 2016, doi: 10.1016/j.phpro.2016.08.148.

[35] Kenneth C Mills, *Recommended Values of Thermophysical Properties for Selected Commercial Alloys*. Materials Park, OH: ASM International, 2002.

[36] D. Deng, K. Ogawa, S. Kiyoshima, N. Yanagida, and K. Saito, "Prediction of residual stresses in a dissimilar metal welded pipe with considering cladding, buttering and post weld heat treatment," *Comput. Mater. Sci.*, vol. 47, no. 2, pp. 398–408, 2009, doi: 10.1016/j.commatsci.2009.09.001.

[37] L.-E. Lindgren, *Computational Welding Mechanics Thermomechhanical and Microstructural Simulations*. New York: Woodhead Publishing, 2007.

[38] K. starr Odum, "Method to reduce final part deformation using thermal control of the directed energy deposition process," University of California, Davis, 2019.